Geophysical Journal International

Geophys. J. Int. (2010) doi: 10.1111/j.1365-246X.2010.04705.x

The Rudbār M_w 7.3 earthquake of 1990 June 20; seismotectonics, coseismic and geomorphic displacements, and historic earthquakes of the western 'High-Alborz', Iran

Manuel Berberian[1] and Richard Walker[2]

[1] *1224 Fox Hollow Drive, Toms River, NJ* 08755-2179, *USA. E-mail: manuel.berberian@gmail.com*
[2] *Department of Earth Sciences, University of Oxford, Parks Road, Oxford* OX1 3PR, *UK. E-mail: Richard.Walker@earth.ox.ac.uk*

Accepted 2010 June 17. Received 2010 June 17; in original form 2008 December 21

SUMMARY

The Rudbār earthquake of 1990 June 20, the first large-magnitude earthquake with 80 km left-lateral strike-slip motion in the western 'High-Alborz' fold-thrust mountain belt, was one of the largest, and most destructive, earthquakes to have occurred in Iran during the instrumental period. We bring together new and existing data on macroseismic effects, the rupture characteristics of the mainshock, field data, and the distribution of aftershocks, to provide a better description of the earthquake source, its surface ruptures, and active tectonic characteristics of the western 'High-Alborz'. The Rudbār earthquake is one of three large magnitude events to have occurred in this part of the Alborz during recorded history. The damage distribution of the 1485 August 15 Upper Polrud earthquake suggests the east–west Kelishom left-lateral fault, which is situated east of the Rudbār earthquake fault, as a possible source. The 1608 April 20 Alamutrud earthquake may have occurred on the Alamutrud fault farther east. Analysis of satellite imagery suggests that total left-lateral displacements on the Rudbār fault are a maximum of ∼1 km. Apparent left-lateral river displacements of ∼200 m on the Kashachāl fault and up to ∼1.5 km of the Kelishom fault, which are situated at the eastern end of the Rudbār earthquake fault, also appear to indicate rather small cumulative displacements. Given the relatively small displacements, the presently active left-lateral strike-slip faults of the western High-Alborz fold-thrust belt, may be younger than onset of deformation within the Alborz Mountains as a whole.

Key words: Seismicity and tectonics; Continental tectonics: strike-slip and transform; Asia.

1 INTRODUCTION

The Rudbār earthquake of 1990 June 20 (M_w 7.3; M_o 1.05 × 10^{20} Nm; I_o IX) is one of the largest, and most deadly, earthquakes in Iran. It affected both urban and rural regions, killed 13 000–40 000 people, and made a further 500 000 homeless. The earthquake is the largest instrumentally recorded event in the Alborz Mountains of northern Iran and was associated with a range-parallel left-lateral strike-slip surface rupture of ∼80 km. The ruptures follow the main ridges of the 'High-Alborz', at altitudes of ∼2900 m, and in regions in which the geology is typified by tight folds and intense reverse faulting (Figs 1–3).

Despite the large magnitude, an extensive meizoseismal area, widespread urban and rural destruction, extremely large death toll, and tectonic importance of the earthquake, identification of the coseismic surface fault was hampered by (i) epicentral error and (ii) conflicting sets of speculative field observations/interpretations of the causative fault. The preliminary field survey of Berberian *et al*. (1992), though still valid, was restricted to a short reconnaissance field trip to the epicentral region. They described three main fault segments, arranged in a right-stepping en-échelon pattern separated by gaps in the observed surface ruptures, with left-lateral strike-slip motion on almost vertical planes. Later studies have attempted to describe the Rudbār earthquake primarily through seismological investigation.

In this study, we provide critical information on the preferred parameters and mechanisms of the coseismic surface rupture, the mainshock and the aftershock tectonics. We report the coseismic surface fault features based on additional field studies that were carried out almost a decade after the earthquake. Field photographs supplement the discussion on the surface rupture. We also analyse details of the spatial and temporal patterns of the pre-1990 medium-magnitude north-dipping thrust events, which might have interacted with the 1990 strike-slip rupture within the seismogenic zone, and eventually loaded and triggered the 1990 earthquake. Furthermore, we discuss the scattered aftershocks, which were observed over a wide area outside the main coseismic rupture zone, and had either strike-slip or reverse mechanisms. It seems that the aftershocks ruptured through the mainshock stepover area (i) in the Sefidrud surface rupture gap and (ii) the compressional stepover area between the

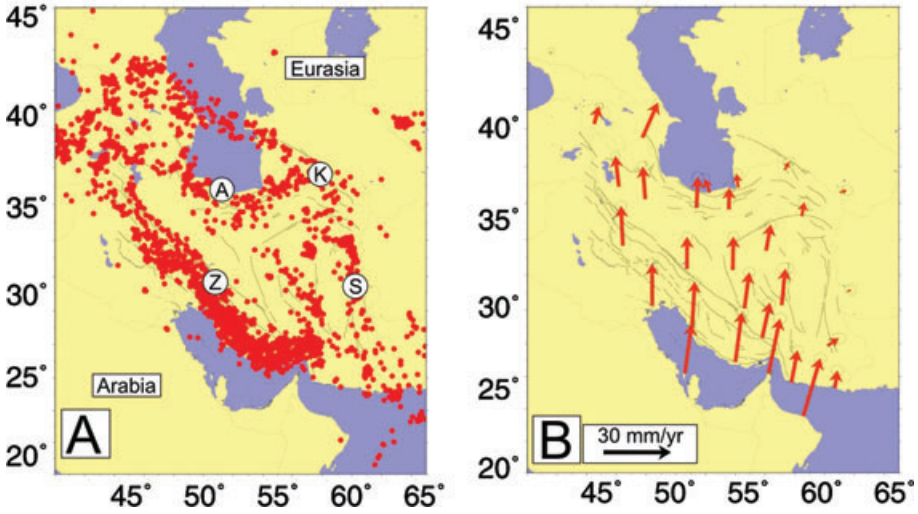

Figure 1. (a) Seismicity of Iran 1964–1998, from the catalogue of Engdahl *et al*. (1998). The Zāgros Mountains in the SW are marked by Z, the Alborz Mountains in the north by A, the Kopeh Dāgh by K, and the Sistān region by S. (b) Map of Iran showing GPS velocity points relative to Eurasia (Vernant *et al*. 2004). The GPS velocities decrease to zero at both the northern (Kopeh Dāgh) and eastern (Sistān) margins of Iran, suggesting that the Arabia–Eurasia convergence is accommodated within the political borders of Iran. Most of the active deformation occurs in the seismically active Zāgros (in the SW and S), Alborz (north, south of the Caspian Sea) and Kopeh Dāgh (NE) mountain.

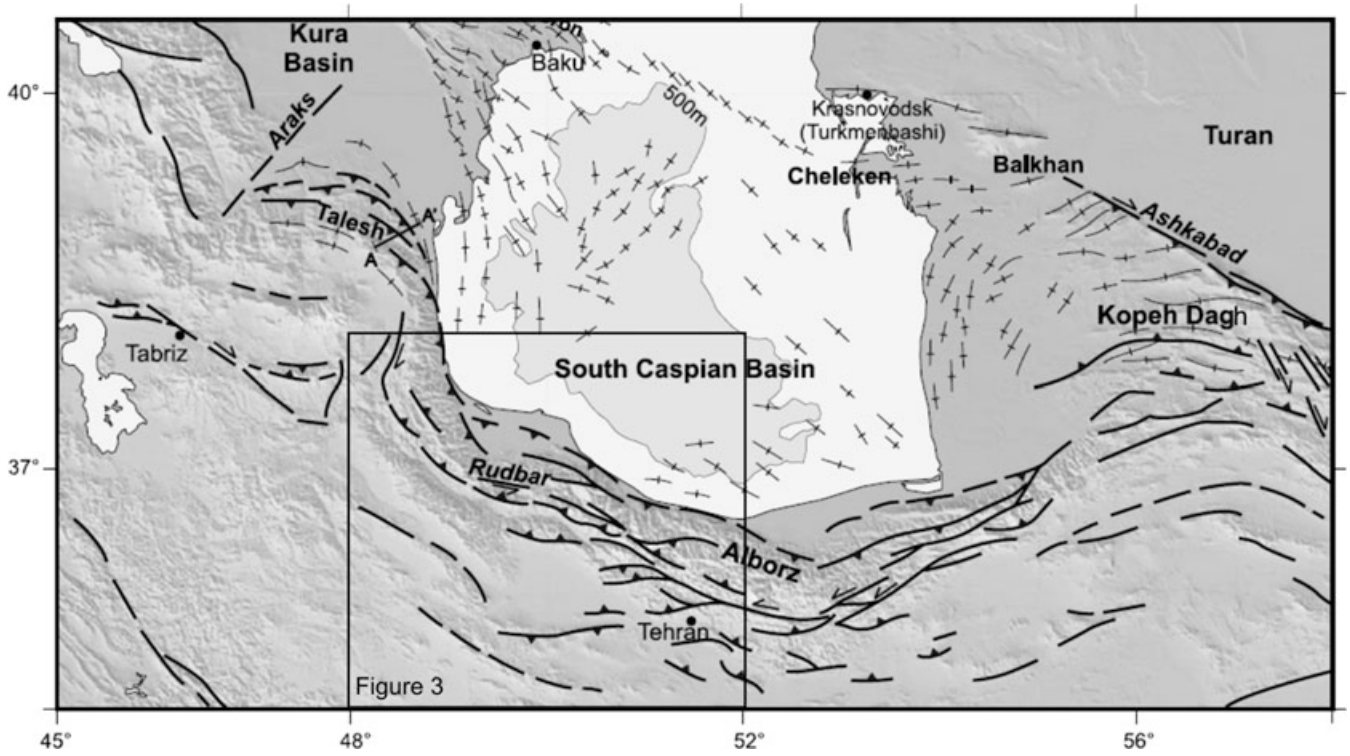

Figure 2. Generalized tectonic map of the South Caspian and surrounding regions showing the major active faults (after Jackson *et al*. 2002). Northern latitudes and Eastern longitudes are marked.

southeastern extremity of the Rudbār fault and the northwestern section of the Shāhrud thrust (Fig. 4). We then introduce, from an analysis of Shuttle Radar Topography Mission (SRTM) digital topography and Advanced Spaceborne Thermal Emission and Reflection Radiometer (ASTER) satellite imagery, the record of cumulative displacements associated with the Rudbār fault and with two other, potentially active, left-lateral strike-slip faults within this part of the 'High-Alborz'. We then discuss the possible association of these faults with newly refined macroseismic data of pre-1900 large-magnitude earthquakes. Associating large pre-instrumental earthquakes with their causative faults is important for understanding regional seismic hazard and potential future fault activity.

Note that in the text, the Persian geographical names and other Persian words are written as they are correctly pronounced and written originally, with direct and simplified transliteration from Persian into English. Diacritical marks and special characters are used to differentiate vowel 'A' [short; e.g. ant] from 'Ā' [long; e.g. Ārmenian] and Arabic 'ain' as 'A' [e.g. 'Abbās]. Where appropriate,

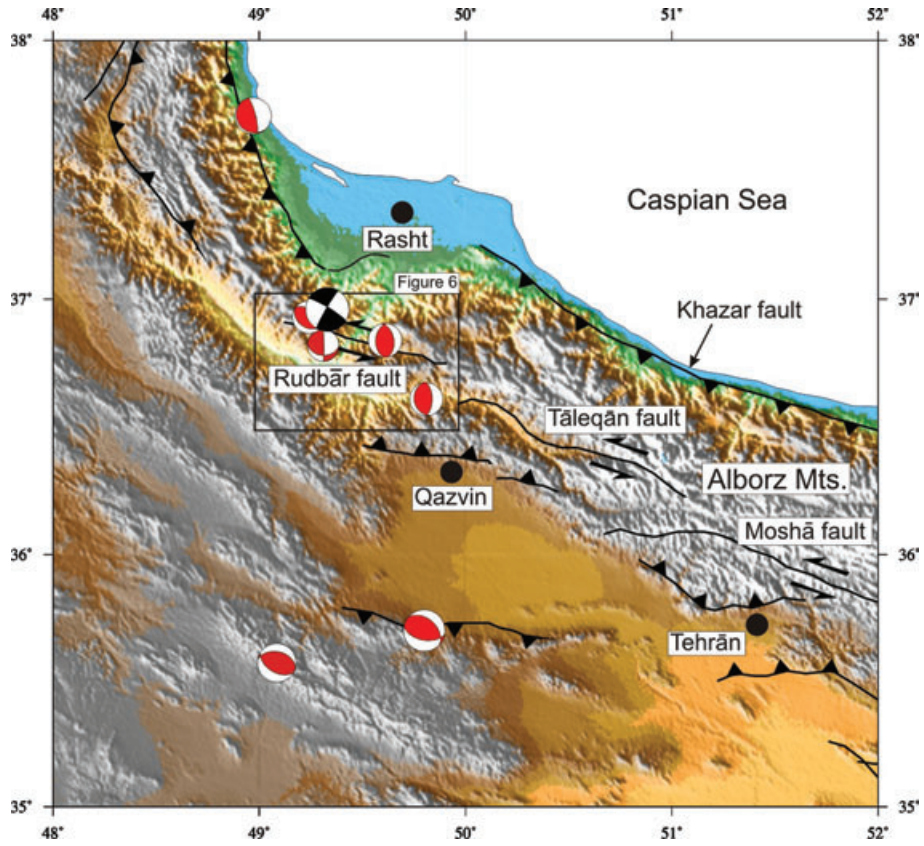

Figure 3. The main active faults (from Berberian & Yeats 1999) and fault-plane solutions of earthquakes (from Jackson *et al*. 2002) in the western Alborz overlain on shaded-relief digital topography. The mainshock of the 1990 Rudbār earthquake is in black to differentiate it from the others. Triangular barbs are on the hangingwall side of the thrusts indicating the dip of thrusts and sense of convergence.

translations are added in brackets. Elevations reported are in metres above the mean sea level (amsl)."

2 GEOLOGY AND TECTONICS OF THE ALBORZ MOUNTAINS

The Alborz is an arcuate fold-and-thrust mountain belt in the north of Iran. It is ∼100 km wide, ∼1000 km long, and curves along the southern margin of the Caspian Sea (Figs 1–3). It includes summits from +3600 to +4800 m in altitude, culminating in Mount Damāvand volcano (35.95°N–52.01°E, +5670 m), which lies approximately in the centre of the mountain belt (Fig. 2). The mean elevation of the Alborz drops from +3000 m in the inner belt to −28 m (bmsl) along the Khazar reverse fault (Berberian 1981, 1983) at the Caspian Sea shoreline in the north. It also drops to approximately +1500 m at its southern margin with North-Central Iran along the Manjil, North Tehrān and the North Qazvin reverse faults in the south and southwest (Berberian *et al.* 1983, 1985, 1992; Berberian & Yeats 1999, 2001). The structural trend of the Alborz changes from N110°E in the western Alborz to N80°E in the eastern Alborz, and a marked hinge occurs near longitude 52.5°E (Fig. 2). There is abundant evidence for recent uplift in the Alborz Mountains in the form of incised river terraces and coastal marine terraces (Berberian 1983). Recent GPS data analysis indicates that north–south shortening across the Alborz occurs at 5 ± 2 mm yr^{-1}, with a left-lateral shear of the overall belt at a rate of 4 ± 2 mm yr^{-1} (Vernant *et al.* 2004). Apparently, the Alborz behaves as a transpressional orogen accommodating the differential motion between Central Iran in the south and the South Caspian Basin in the north (Jackson *et al.* 2002). Ritz *et al*. (2006) suggest that the Taléqān and Moshā left-lateral faults of the western Alborz (Fig. 3) have accommodated a component of extension since the middle Pleistocene (∼1–1.5 Ma). This extension, which is confined to high parts of the range, is possibly related to the motion of the South Caspian Basin.

The Sefidrud [lit. 'White River'; the ancient/pre-Sāssāniān-AD 224- 'Amārdus' River], which transects the 1990 earthquake meizoseismal area (Figs 4 and 5), is the only river of any size to cross the Alborz Mountains from Central Iran in the south to the Caspian Sea in the north. It passes through a deep gorge at Rudbār at ∼36.80°N–49.40°E in the centre of the epicentral region of the 1990 earthquake (Figs 4 and 5). The Sefidrud, with a 370 km long course, high alluvial load, and strong erosive power, appears to have cut a water gap through the 'High-Alborz', and has captured the catchments of the Qezel Owzan River [lit. 'Great River'] that runs from NW to SE for >150 km, and the Shāhrud [lit. 'King/Mighty River'] that runs from ESE to WNW for >140 km (Fig. 4). The Shāhrud and Qezel Owzan Rivers join together in the Manjil area, south of Rudbār town and the Manjil thrust, where the Sefidrud buttress gravity dam was constructed from 1958 to 1962 at the entrance of the deep gorge on the Manjil thrust (Figs 4 and 5). The Sefidrud gorge has a long record of human habitation as shown by the Mārdes/Amārdes culture, which flourished in the region in the Bronze and the Early Iron Age around the end of the second Millennium B.C. (Hākemi 1968; Negahbān 1968, 1990; Haerinck 1989).

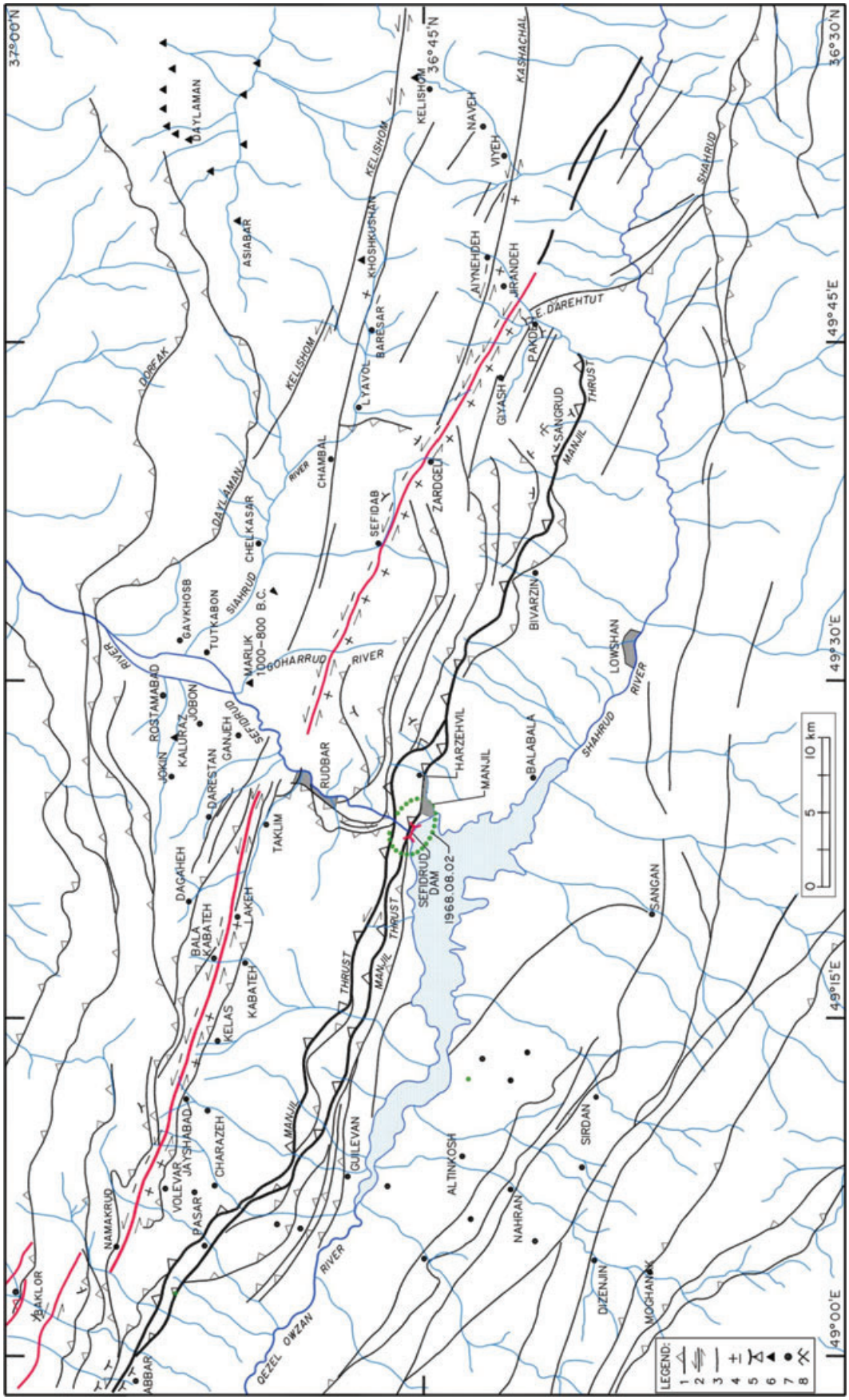

Figure 4. General fault map of the area and locations referred in the text. Legend: (1) Thrust fault. (2) Left-lateral strike-slip fault. (3) Fault without specification. (4) Vertical motion ('+' and '−' symbols denote the uplifted and down-dropped sides of the fault). (5) Landslide and rockfall. (6) Archaeological sites. (7) Village. (8) Mine.

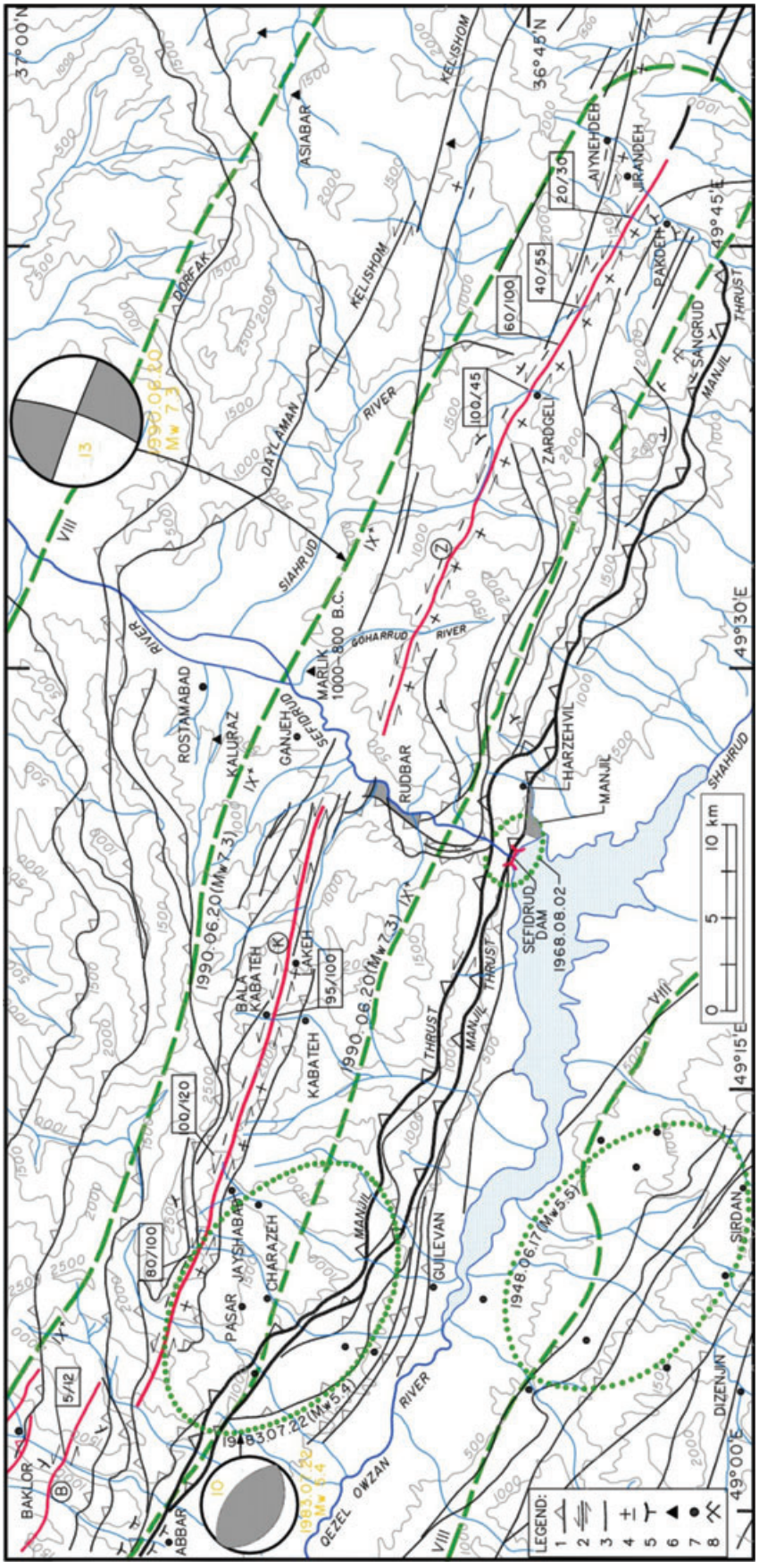

Figure 5. Seismicity, fault, and topographic map of the Rudbār area in the western Alborz Mountains. The revised 1990 June 20 Rudbār earthquake surface rupture are drawn in red: the coseismic horizontal/vertical displacements (in cm) are given in boxes. The isoseismal area (green broken lines) and the post-1900 seismicity (for events in 1968 August 22, 1948 July 17 and 1983 February 22) of the Rudbār area are demonstrated. Three main segments of the surface rupture are labelled by red encircled letters (from the NW to the SE) as B: Baklor, K: Kabateh, and Z: Zardgeli. Fault plane solutions for the 1990 June 20 mainshock are from Gao & Wallace (1995) and from Priestley *et al.* (1994) for the 1983 July 22 event. The creation of the unique Sefidrud River gorge, which is the only river crossing the ~1000 km length of the Alborz Mountain, and which also acted as a major barrier during the 1990 earthquake, may have been facilitated by the segment boundary in the NNE–SSW faulting in the Rudbār area. Topographic contour lines are in meters above mean sea level. Additional symbols as in Fig. 4.

3 THE 1990 JUNE 20 RUDBĀR EARTHQUAKE

3.1 Macroseismic effects

The 1990 Rudbār earthquake killed 13 000–40 000, injured 105 000 and left 500 000 homeless. It demolished the towns of Rudbār (36.81°N–49.41°E, +196 m; located in the rupture gap zone, immediately to the south of the coseismic fault line); Manjil (36.73°N–49.38°E, +300 m; 10 km SSW of the fault); Harzehvil (36.73°N–49.43°E, +529 m; 8 km SSW of the fault); and Lowshān (36.61°N–49.50°E, +331 m; 18 km SSW of the fault) (Figs 4 and 5). It also damaged the provincial capital city of Rasht (37.26°N–49.58°E, +0.9 m; 50 km NNE of the coseismic fault; Fig. 3). More than 100 000 houses in 700 villages were destroyed, and 300 additional villages and many towns sustained some damage. Almost 1300 schools with 7000 classrooms in two provinces were destroyed or damaged beyond repair (Berberian *et al.* 1992).

As with the Bam earthquake of 2003 (e.g. Berberian 2005) healthcare facilities and infrastructure were badly affected. The Rudbār two-story hospital built in 1987 at a cost of Rls 600 million (∼US$ 500 000.00) and the Rostamābād hospital (36.88°N–49.48°E, +155 m; 9 km NE of the coseismic fault) were demolished, along with a further 85 healthcare centres and hospitals in two provinces (Figs 4 and 5). Some villages lost up to 80 per cent of their livestock. The damage to engineering structures was in the form of rockfalls and landslides over highways and roads; collapse of portions of tunnels, building collapses due to liquefaction; extensive damage to equipment in many industrial facilities including a major cement plant; damage to a power plant; damage to non-structural elements in residential and office buildings; minor cracks in a major concrete buttress dam built on the Manjil thrust; and minor damage to a modern grain silo. The earthquake completely demolished the underlying economic infrastructure in two provinces of Gilān and Zanjān. The earthquake took place two years after the 8-yr Iran–Iraq war, when the country was in deep hardship and was not prepared for another manmade disaster of this scale. Direct economic loss was estimated to be US$ 7.2 billion (original values), approximately 2.5 per cent of GPD (UNDRO 1990a,b,c; Āstāneh & Ghafory-Ashtiāny 1990; Underwood 1991; Berberian *et al.* 1992; Berz 1992).

3.2 Mainshock

The plot of the epicentral locations of the mainshock by different agencies (Table 1) and some of the aftershocks to the north of the coseismic left-lateral strike-slip surface fault is a matter of interest (Fig. 6). As will be discussed later in the text (Sections 3.3.1.a, and 4) and documented by the field photographs (Figs 7–9), the surface rupture of the Rudbar strike-slip fault shows a nearly vertical dip. No other strike-slip fault is present at the surface in the telesismically recorded mainshock area (Figs 4–6). There is no evidence to suppose a nearly vertical fault at depth about 10 km to the north of the 1990 coseismic surface rupture and assume a connection to the surface rupture 10 km to the south. This assumption violates the intensity distribution, which unlike the fault data, was carefully recorded at the surface immediately after the event (Fig. 5).

The distance between the epicentres relocated by Engdahl *et al*. (2006) and Gao & Wallace (1995) is a few kilometres, but both locations are 10 km to the northeast of the coseismic surface rupture. The 10–15 km systematic distance between the post-1970s epicentral locations of large-magnitude earthquakes and vertical coseismic surface faults has been typical for earthquakes in Iran (Ambraseys 1978, 2001; Berberian 1979; Berberian *et al*. 1992; Engdahl *et al.* 2006). We speculate that the systematic bias in the Iranian teleseismic earthquake locations is mainly introduced by deviations in traveltimes from globally averaged velocity models

Table 1. Teleseismic parameters of the 1990 June 20 Rudbār Mainshock (with left-lateral strike-slip coseismic surface faulting) arrange by the computed origin time.

Origin Time (GMT)	Epicentre (N°–E°)	m_b	M_s	M_w	Depth (km)	rms (s)	Source[a]	Distance of epicentre from the fault (km)
21:00:07.1	36.93–49.50	6.7	7.1		03.0		MOS	13 NE
21:00:08.5	36.96–49.41				10.0		UNK	15 NE
21:00:09.9	36.95–49.40	6.4	7.7	7.3	18.5	1.21	NEIC	13 NE
21:00:10.3	37.07–49.23	6.5	7.9		10.0		BJI	15 NE
21:00:10.8	36.98–49.34	6.2	7.4		18.5f	1.34	ISC	13 NE
21:00:12.3	36.99–49.22	6.2	7.4	7.4	12.0	1.67	E *et al.* 2006	10 NE
21:00:12.7	36.96–49.32	6.2		7.3	18.3	1.87	EHB, 1998	10 NE
21:00:13.0	37.00–49.40	6.2			33.0		NAO	15 NE
21:00:13.1	36.49–49.24[b]				10.0		TEH(IGTU) [1990 June 25]	42 SW
21:00:13.1[c]	36.82–49.41[d]	7.3			10.0		TEH(IGTU)	[Fixed at Rudbar]
21:00:19.1	36.97–49.30				76.0		CSEM	10 NE
21:00:2[e]	36.82–49.41[d]	7.3			10.0		TEH(IGTU)	[Fixed at Rudbar]
21:00:27.0	38.30–47.80	5.8	7.0				HFS	193 NW
21:00:31.1	36.95–49.52				15.0f		HRVD	13 NE
–	36.96–49.34						G&W, 1995	11 NE

Notes: [a]MOS: Moscow, Geophysical Survey of Russian Academy of Sciences, http://www.gsras.ru/. UNK: Unknown source (reported by ISC). NEIC: National Earthquake Information Center. U.S. Geological Survey, http://neic.usgs.gov/. BJI: Institute of Geophysics, Earthquake Administration, Beijing, China. ISC: International Seismological Centre, http://www.isc.ac.uk. E *et al.* 2006: Engdahl *et al.* (2006). EHB: Engdahl *et al.* (1998). NAO: NORSAR, http://www.norsar.no/. TEH (IGTU): Institute of Geophysics, Tehran University (IGTU), http://irsc.ut.ac.it/. CSEM: Centre seismologique Euro-Mediterraneen, http://www.emsc-csem.org. HFS: Hagfors Observatory, Sweden. HRVD: Centroid Moment Tensor Catalogue, Harvard University, http://www.seismology.harvard.edu/cmtsearch.html. G&W, 1995: Gao & Wallace (1995).

[b]Location announced five days after the event by the Institute of Geophysics, Tehran University.

[c]Reported by Tsukuda *et al.* (1991).

[d]Fixed manually by the coordinate location of the destroyed town of Rudbār.

[e]Reported by ISC.

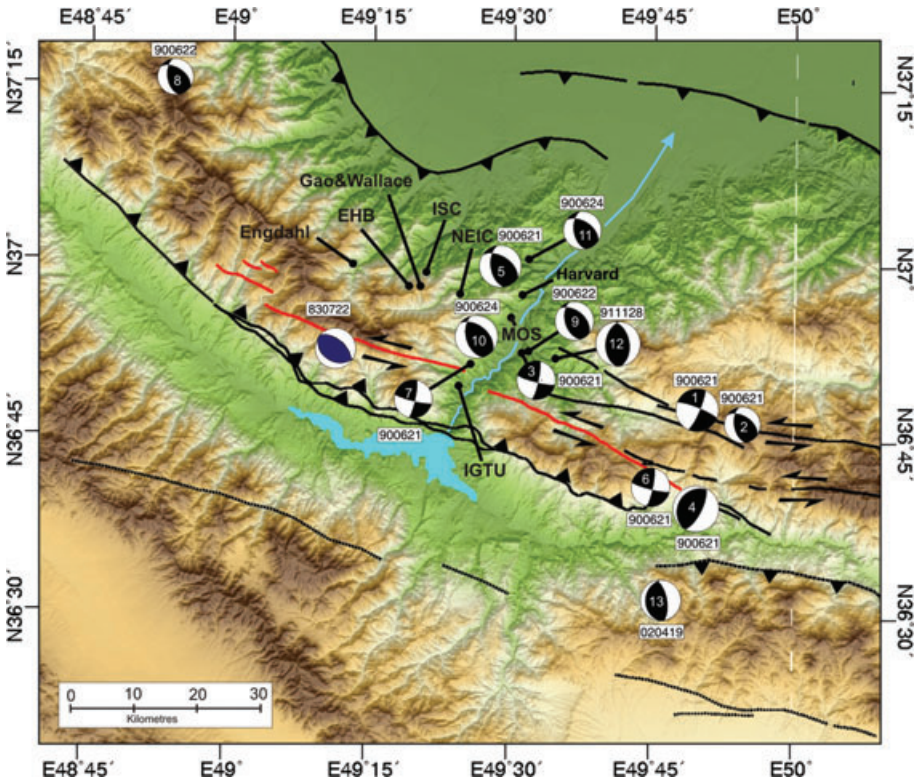

Figure 6. Focal mechanism solutions of the Rudbār earthquake aftershocks (Gao & Wallace 1995: See Table 3 for the seismic parameters of the major aftershocks). The fault-plane solution of the 1983 Charazeh earthquake (Priestley *et al*. 1994) is also included, but coloured blue to differentiate it from the aftershock fault-plane solutions (black). The 1990 mainshock epicentre, determined teleseismically by different agencies and individuals, are shown by black dots. EBH: Engdahl *et al*. (1998). Engdahl: Engdahl *et al*. (2006). Gao & Wallace: Gao & Wallace (1995). HRVD: Harvard University. IGTU: Institute of Geophysics, Tehrān University. ISC: International Seismological Centre, UK. MOS: Geophysical Survey of the Russian Academy of Sciences, Moscow. NEIC: National Earthquake Information Centre, USGS, Colorado. The 1990 earthquake coseismic surface rupture is in red. Blue: The Sefidrud dam reservoir (the concrete buttressed gravity dam was built on the Manjil thrust fault in 1962; see Fig. 4). This, and all later maps, are in UTM zone 39.

and asymmetric/inadequate azimuthal distribution of recording stations. The typical location error values of 10–15 km for the post 1970s large-magnitude Iranian earthquakes have precluded correct identification of the causative faults.

In their inverted source model, Campos *et al*. (1994) and Virieux *et al*. (1994) defined nine subevents over the first 25 s with lateral heterogeneities in the source region (Table 2). These nine events describe an initial bilateral rupture, with both northwestern and southeastern propagation during the first ten seconds. This is then reduced to unilateral, southeastward rupture propagation for the last part of the source excitation. The bilateral rupture extended about 20 km to the northwest and about 60 km to the southeast of the epicentre for a total fault length of about 80 km, rupture azimuth of N120°E, compatible with the point source focal mechanism, and at a rupture velocity of 2.5 km s^{-1}. Each subevent has a simple time function with a total duration of 4s and a rise time of 2s.

We consider the relocated epicentre location of Engdahl *et al*. (2006) as the approximate 'longitude' of the initial rupture propagation point (±10 km), and simply slide it southwards reaching the coseismic surface fault line. This puts the location of the main shock subevent I nucleation point of Campos *et al.* (1994), which generated 13.3 per cent of the total scalar moment release, somewhere close to Jayshābād on the Kabateh fault segment (Fig. 5). This location demonstrated about 100 cm left-lateral, and 120 cm vertical coseismic displacements on a nearly vertical fault plane, and is close to the 1983 July 22 M_w 5.4 thrust event (Fig. 5, Tables 2 and 4). Taking into consideration of the modelling results of Campos *et al.* (1994), the coseismic rupture propagated bilaterally 20 km to the NW of the epicentre (subevents 1–3), and 20 km to the southeast (subevents 4 and 5). These five subevents cover the Kabateh and the Baklor surface ruptures west of the Sefidrud gap, with subevent 3 at the western tip of the Baklor rupture (Fig. 5). Subevent 6, generating 22 per cent of the total scalar moment release, starts near the western portion of the Zardgeli segment to the east of the Sefidrud gap. The last Subevent 9, generating the lowest scalar moment release of 3.5 per cent, coincides with the termination point of the coseismic surface rupture at the southeastern extremity of the Zardgeli segment. The 20 km additional rupturing deduced from the inversion procedure of the broadband data (subevents 3 and 9) has definitely not reached the surface.

Campos *et al.* (1994) reported that subevents 1, 2 and 3, located in the western fault segment, had strike-slip mechanism with nearly vertical planes dipping north and a slight normal-slip component. These mechanisms are slightly different from those subevents located to the east of the nucleation point (subevents 4–9), which represented a minor reverse component of slip. This seems to be in agreement with the deformation recorded along the coseismic surface fault line. Subevents 1–3 are located on the western section of the Kabateh as well as the Baklor segments, where slight local normal slip component is observed on the ground with the southern block downthrown (Figs 7a–c). To the east of subevent 1, around Jayshābād (Fig. 5), a reverse slip component is more prevalent (Figs 8a,b, 9a and b).

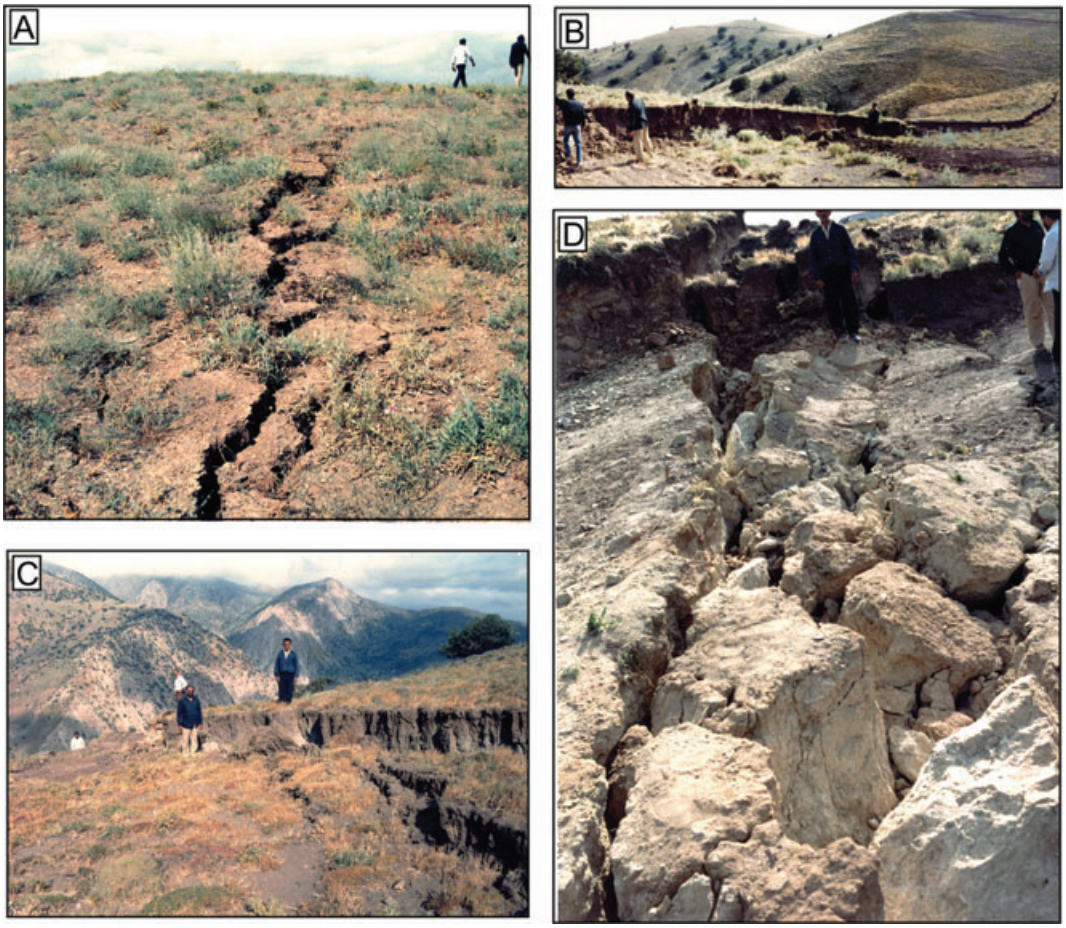

Figure 7. (a) Small left-lateral displacement and uplift of the southern (left) block along the Baklor segment (see Fig. 4 for the location of the segment). South of the Baklor village View to the WNW. (b) Coseismic rupture with NNE-facing scarp along the Kabateh segment, near Jayshābād (west of the Kelās ravine). The southern block (left) is uplifted against the northern (right) higher topography. Left-lateral displacement of 100 cm and vertical motion of 120 cm were recorded in this area. View to the west. (c) Closer view of the Kabateh segment near Jayshābād (west of the Kelās ravine), with some normal slip. The southern block (right) is uplifted against the northern block (left) along a nearly vertical left-lateral slip fault. View to the east (All photographs are from June 1990).

Choy & Zednik (1997), examined a slightly extended bandwidth with higher frequencies than those used by Campos *et al.* (1994). They also did not low-pass the data and did not incorporate *SH* waves in their waveform analysis of the mainshock. Their mainshock solution consisted of a tiny precursory subevent followed after twenty seconds by a series of four subevents with left-lateral strike-slip mechanism, depth ranging from 10 to 15 km, and rupture length of about 60 km (Table 2). The first major subevent nucleated slightly to the NW of the initial precursor and occurred about 9 s after the initial minor precursory subevent. The second subevent occurred slightly south of the initial precursor. These subevents are located to the west of the Sefidrud gorge. The last two subevents, located to the east of the Sefidrud gap, moved progressively southeastward of the first subevent.

By considering the same process applied above for the previous modelling, the modelling result of Choy & Zednik (1997) would appear to violate the Sefidrud gap along the coseismic surface rupture, though with the uncertainties in location this apparent violation might not be real. In order to include the Sefidrud gap, we have to shift the 'initial precursory event' of Choy & Zednik (1997) about 8.5 km to the east of Jayshābād and locate it at Bālā Kabateh (Fig. 5). In this case, subevents 1 and 2 would be located to the west of the Sefidrud gap, on the Kabateh segment, and subevents 3 and 4 to its east on the Zardgeli segment. Furthermore, the overall rupture zone from the modelled four subevents gives a length of about 60 km, versus the coseismic surface rupture of 80 km and the total fault length of 100 km modelled by Campos *et al.* (1994) and Virieux *et al*. (1994). All the models show shorter initial rupture propagation to the NW followed by longer rupture propagation towards the SE.

3.3 Aftershocks

The mainshock was followed by a large number of small-magnitude aftershocks (Fig. 6). Some medium-magnitude aftershocks were teleseismically recorded. Aftershocks which occurred 2, 6, 13 and 16 hours after the mainshock, as well as the one on June 24 added to the destruction. They increased the casualties and caused landslides and rockfalls that further blocked the access roads leading to the stricken areas. The relocation of $M_s > 4.6$ aftershocks of 1990 June 21–1990 June 24, using the joint hypocenter determination method (JHD89, Dewey 1971, 1983), gave a better locations with a NW–SE direction (Gao & Wallace 1995).

3.3.1 Telesismically recorded aftershocks

Single station inversion of the broadband records of $M_s > 4.6$ aftershocks within the first 3 d (Gao & Wallace 1995), as well as the *P*/*SH* Body waveform modelling of the 1991 (Jackson *et al.* 2002)

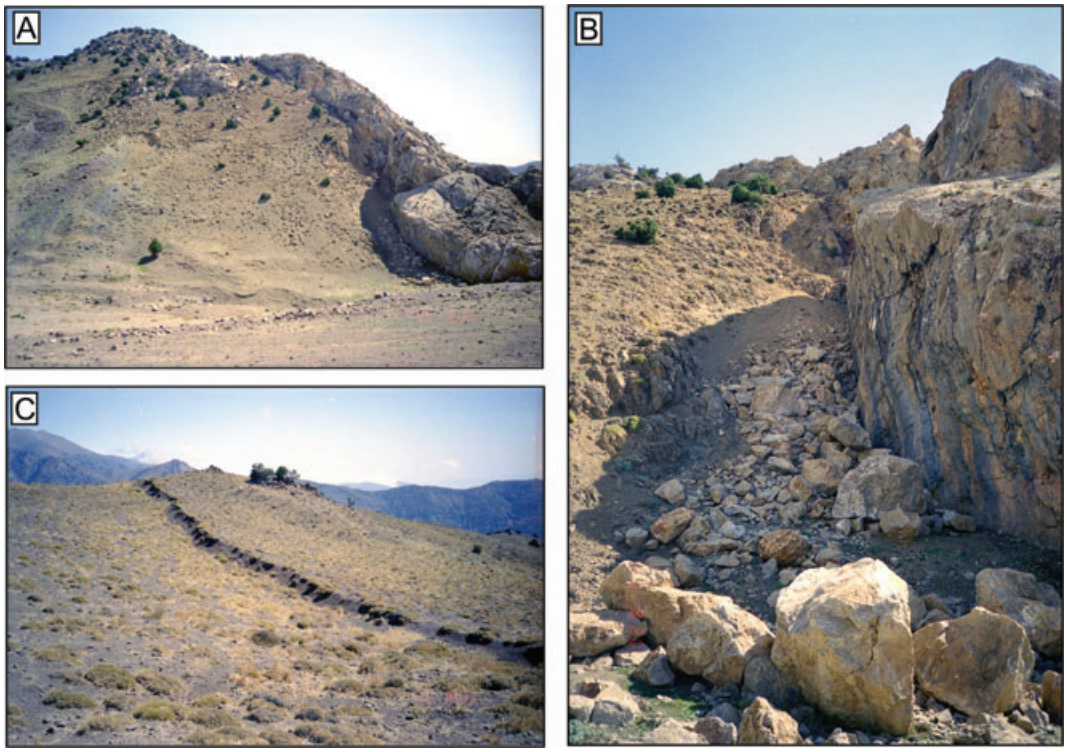

Figure 8. (a) General view of the NNE-facing, nearly vertical (slightly dipping SSW) Kabateh segment fault scarp of the Rudbār earthquake fault, eastern flank of the Kélās ravine (∼36.75°–49.16°E; east of Jayshābād, west of Kabateh). The southern block (right: composed of the Late Jurassic-Early Cretaceous limestone) has been uplifted against the northern block (left; the dark to black Eocene-Oligocene shale, sandstone and volcanic tuff) against the existing topography of the High-Alborz. View to the SSE. (b) Close-up view of the Kabateh segment of the Rudbār fault with nearly vertical (slightly dipping SSW) fault plane shown in 'a'. The 1990 coseismic vertical displacement was about 1.2 m at this locality. The rest of the fault scarp [total height varying between 6 to 10 m] is formed during the past earthquakes and erosion of the northern (left) block. View to the SE. (c) North-facing coseismic fault scarp in the area between Kélās and Jayshābād (36.90°N–40.16°E, +1951 m). The southern block (right = south; with general lower topography) is raised against the general higher topography of the High-Zagros (left = north). Left-lateral displacement of 80 cm and vertical motion of 100 cm were recorded in this area. View to the SE (All photographs taken in September 2000).

and the 2002 April 19 events (HRVD-CMT; ZUR-RMT) resulted in both pure strike-slip and pure reverse/thrust focal mechanisms (Table 3 and Fig. 6). This is consistent with slip partitioning into pure strike-slip and reverse-slip earthquakes. Slip vectors of the mainshock and some aftershocks are perpendicular to the general direction of the nearly N–S shortening in the Alborz, while the rest are in a general NE–SW direction. Despite differences in the slip vector trends of the strike-slip and thrust aftershocks, in general, the directions of the *P*-axes are consistently to the NE (Berberian *et al.* 1992; Gao & Wallace 1995; Berberian 1997; Choy & Zednik 1997; Jackson *et al.* 2002).

Left-lateral strike-slip aftershocks. Body waveform modelling of the four aftershocks of 1992 June 21 (02:08 GMT, M_s 4.9; 07:50 GMT, M_s 4.9; 21:27 GMT, M_s 4.9 and 21:31 GMT, M_s 4.8) show left-lateral strike-slip mechanism on WNW–ESE striking nearly vertical faults (Table 3 and Fig. 6), consistent with the mainshock (Gao & Wallace 1995). Three aftershocks, which took place at 02:08 GMT, 07:50 GMT and 21:27 GMT, are located along the Zardgeli segment of the coseismic surface rupture, to the east of the Sefidrud gap, and with source parameters showing a dip of 80° to the SE,of the Zardgeli fault segment and 81° in the NW. These observations do not agree with the presence of a 45° north dipping fault at the NW and centre of the Zardgeli fault segment, progressively changing to 90° dip at its SE extremity, as suggested by the microseismicity data of Tatar & Hatzfeld (2009). The observations also do not appear to agree with the interpretation of Gao & Wallace (1995) that the 1990 May 21 (21:27 GMT) aftershock took place on the eastern bend of the Manjil thrust with right-lateral strike-slip mechanism. Both Gao & Wallace (1995) and Niāzi & Bozorgniā (1992), influenced by Moinfar & Nāderzādeh (1990) who misidentified landslides as coseismic surface faults, erroneously considered the Manjil thrust as a right-lateral strike-slip fault.

The fourth strike-slip aftershock (Table 3), with mechanism showing 81° dip on a WNW–ESE trending fault, took place at the eastern extremity of the Kabateh segment west of the Sefidrud gap. The main shock took place on the centre of this segment near Jayshābād (Fig. 4), with *P*/*SH* body waveform modelling showing 88° dip (Gao & Wallace 1995). It is in this section that a nearly vertical reactivated fault scarp is exposed cutting the Late Jurassic–Early Cretaceous limestone for a length of 15 km (Fig. 8). Knowing the uncertainties in the epicentre locations, the mapped coseismic surface rupture, and the focal mechanisms, we may conclude that:

(i) body waveform modelling of the main shock and the four aftershocks imply a dip range of 88° to 80° with a depth range of 13 to 8 km for the coseismic surface rupture of the Rudbār earthquake,

(ii) given the uncertainties in earthquake location, and knowing the focal mechanism and location of surface faulting, the calculated epicentres of the main shock and at least the left-lateral strike-slip aftershocks are presumably shifted towards the northeast, away from the coseismic surface rupture line.

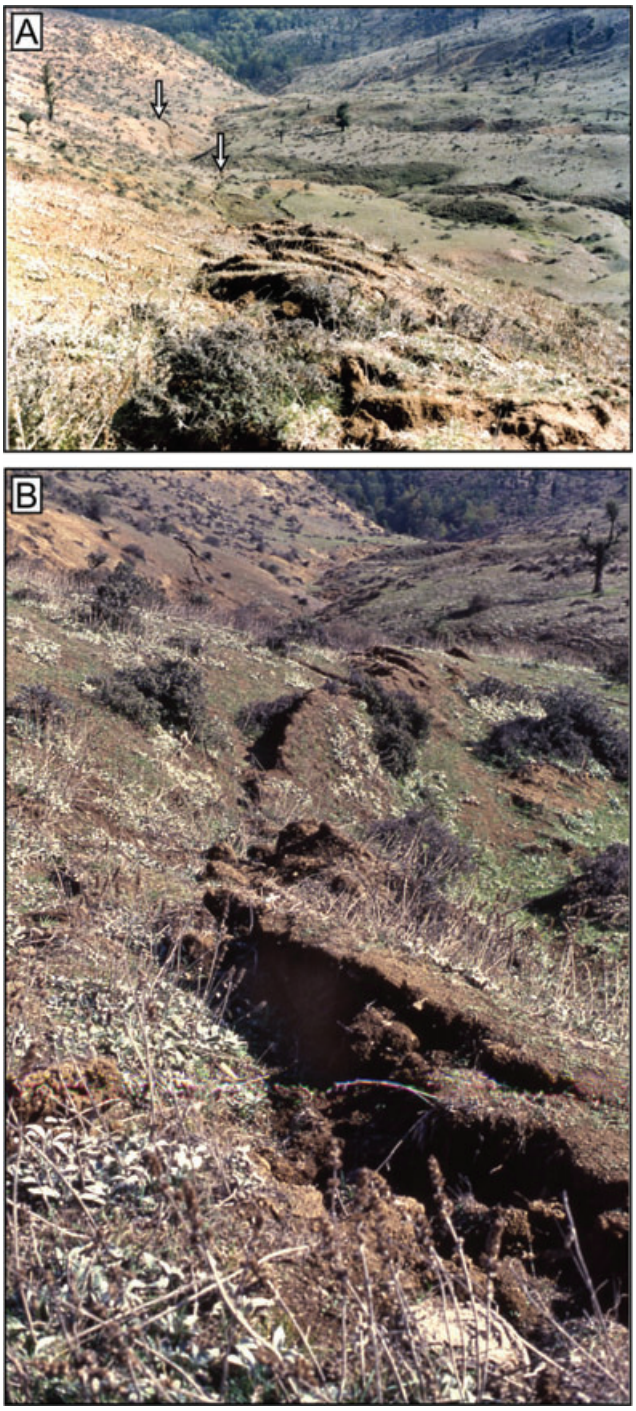

Figure 9. (a) A series of push-ups (mole-tracks) formed by a reverse or thrust component associated with a left-lateral strike-slip along the Zardgeli segment, near Zardgeli. View to the SE. The southern block (right) is raised and upthrust relative to the northern (left) block, against the existing topography. White arrows point to the ruptures in the mid- and far-distance. Left-lateral displacement of 60 cm and vertical motion of 100 cm was recorded in this area. (b) A close-up view of the series of push-ups in the mid-distance of 'a'. View to the SE (Photographs taken in June 1990).

The mainshock epicentre error ranges from 10 km (Engdahl *et al.* 2006) to 13 km (ISC and NEIC) to the northeast of the coseismic surface rupture. The mainshock epicentres computed by Engdahl *et al.* (2006) and ISC/NEIC require 50° and 45° dips, respectively, for the coseimic fault rupture at a depth of 13 km, which cannot be warranted.

Reverse/thrust aftershocks. The N110°E left-lateral strike-slip coseismic surface faulting of the Rudbār earthquake took place in the 'High-Alborz' dominated by intense folding, thrust faulting, and nappe tectonics, and very close to the 1983 February 22 M_w 5.4 Charazeh earthquake with reverse mechanism. The mainshock was followed by nine aftershocks, with mechanisms constrained by body waveform modelling, showing thrust faulting (Table 3 and Fig. 6). These aftershocks were located in the far NW, at the Sefidrud gap area, and to the SE of the Zardgeli segment (see below). The nodal plane orientations of the regional thrust earthquake focal mechanisms are very consistent with the NW–SE striking thrust faults with minor left-lateral oblique strike-slip motion. Except for the two thrust aftershocks of 1990 June 21 and 2002 April 19, which took place to the south of the coseismic surface rupture, the seven remaining aftershocks were located to the north of the surface rupture of the mainshock.

(1) *The Far Northwestern Thrust Aftershock:* The 1990 June 22 (06:07 GM) aftershock is located beyond the meizoseismal area of the mainshock, about 58 km (NEIC; Gao & Wallace 1995) and 35 km (Engdahl *et al.* 2006) to the NW of the meizoseismal area of the 1983 July 22 (∼36.90°N–49.19°E, M_w 5.4; $h = 10$ km) Charazeh earthquake with thrust mechanism (Table 3; Figs 5 and 6). The epicentre of this aftershock is located on the hanging-wall of the Manjil thrust, about 20 km (NEIC; Gao & Wallace 1995) and 17 km (Engdahl *et al.* 2006) to the northeast of the Manjil thrust line. Waveform modelling of this aftershock shows two nodal planes trending NW–SE dipping NE, parallel to the Manjil thrust, and NNW–SSE dipping WSW (Gao & Wallace 1995). Assuming the former being the fault plane, this aftershock may indicate reactivation of the Manjil thrust dipping NE, about two days after the mainshock. Based on the microseismicity, recorded 8 yr after the event, Tatar & Hatzfeld (2009) recommend a 45° dip to the north for the Manjil thrust. Assuming 10 km ± 4 km centroid depth for the 1983 July 22 Charazeh earthquake (Berberian *et al.* 1992; Priestley *et al.* 1994; Jackson *et al.* 2002), and its centre of meizoseismal area at 36.90°N–49.19°E (Fig. 5) being 5 km to the northeast of the Manjil thrust, the dip of the fault would be around 63° towards NE.

(2) *Thrust Aftershocks in the Sefidrud Rupture Gap Area:* Of nine aftershocks with thrust mechanism, five are located in the general Sefidrud deep gorge area, where there was a gap in the coseismic strike-slip surface faulting, as well as to the north of the coseismic strike-slip surface rupture (Table 3; Figs 5 and 6). Except for the 1991 November 28 event, all the four 1990 thrust aftershocks show two systematic nodal planes of NW–SE dipping NE and NNW–SSE dipping WSW (Fig. 6). Several NW–SE trending thrust faults dipping NE are mapped in the area north of Bālā Kabateh (Fig. 4) approaching the Sefidrud gorge, and these aftershocks may indicate their reactivation.

The 1990 June 24 (09:45 GMT, M_w 5.3) aftershock caused additional damage in Rostamābād located in the Sefidrud deep gorge, 9 km to the NE of the coseismic surface fault rupture and triggered landslides blocking the highway passing through the gorge north of Rostamābād (Fig. 5). The Manjil (36.73°N–49.40°E) and the Ābbar (36.92°N–48.97°E) accelerograms recorded peak ground accelerations of 414.65 and 50.31 cm s^{-2}, respectively for the 1990 June 24 aftershock (http://www.bhrc.ac.ir). The high recorded acceleration at the Manjil site as well as a small ellipse showing 90 per cent confidence level of the epicentral location (Gao & Wallace 1995)

Table 2. Source parameters of the 1990 June 20 Rudbār Mainshock (21:00 GMT) (Figs 3 and 6).

Source	M_w	Strike (°)	Dip (°)	Rake (°)	Slip Vector (°)	Centroid Depth (km)	M_o (Nm)
NEIC[a]		311	76	54	112	17	1.1×10^{20}
NEIC[b]		288	88	−11		19	2.0×10^{20}
HRVD[c]		300	73	32	110	15f	1.4×10^{20}
Gao *et al.* 1991[d]	7.2	292	88	−4	112	14	8.8×10^{19}
Berberian *et al*. (1992)[e]	7.3	292	88	−9	112	14	8.8×10^{19}
Campos *et al*. (1994)[f]		300	75	15		5–10	1.2×10^{20}
Campos *et al*. (1994)[g] [9 subevents]		301	81.6	4.8	120	11.7	1.05×10^{20}
		302	78.4	−6.9		11.1	1.67×10^{19}
		2- 295.1	81.4	−15.3		11.6	0.62×10^{19}
		3- 302	88.3	−7.2		14.4	1.14×10^{19}
		4- 304.9	68.3	24.6		9.9	0.69×10^{19}
		5- 307	79.4	16.7		12.5	1.31×10^{19}
		6- 298.3	79.1	4.3		10.7	2.75×10^{19}
		7- 298.6	78.8	9.7		5.6	2.63×10^{19}
		8- 323.3	83.6	28.7		4.4	1.30×10^{19}
		9- 330.5	98.6	46.1		10.9	0.44×10^{19}
Giardini *et al*. (1994)[c]	7.4					10	1.56×10^{20}
Gao & Wallace (1995)[h]		288	88	−9	112	13	1.4×10^{20}
Choy & Zednik (1997)[i] [4 subevents]		1- 285	86	−5		10	1.4×10^{20}
		2- 290	90	−5		12	
		3- 295	90	5		12	
		4- 285	95	5		15	
Sarkar *et al*. (2003)		S1- 298[j]	90[j]	67[j]			
		S2- 300	74	−9		19	
		S3- 290	68	−15			

Notes. See footnotes to Table 1 for expansion of acronyms used here.
[a]Best double couple.
[b]Fault-plane solution, *P*-waves.
[c]Centroid moment tensor solution (Dziewonski *et al.* 1991).
[d,e,f]Long-period surface waves.
[g]Body waves for a point source model (m6 model).
[h]Body wave modelling.
[i]Did not incorporate *SH* waves.
[j]Foreshock (Sarkar *et al.* 2003).

puts this aftershock near the Sefidrud deep gorge (Figs 5 and 6, Table 3).

During the 1991 November 28 event (17:19 GMT, M_w 5.7), which had a nearly N–S thrust mechanism derived from *P*/*SH* body waveform modelling (Jackson *et al.* 2002), one person died, 70 were injured, and the gas–electricity–water supply was damaged at Rudbār and Rostamābād (both located in the Sefidrud gorge; Figs 4 and 6, Table 3). Damage to the gas supply system triggered a fire at Rostamābād. Scores of houses reconstructed after the 1990 earthquake were damaged by this aftershock, and landslides blocked the roads. The Sefidrud Dam-2 and Dam-4 (36.75°N–49.39°E), the Rudbār (36.80°N–49.40°E), and the Daylamān (36.68°–49.90°E) accelerograms recorded peak ground accelerations of 444.70, 138.43, 280.51, and 9.75 cm s^{-2}, respectively for the 1991 November 28 aftershock (http://www.bhrc.ac.ir). Damage and strong motion data indicate that the aftershock was located along the Sefidrud gorge. The ISC and NEIC epicentres are located about 6 km to the east of the gorge. Some nearly N–S superficial thrust faults dipping west are visible in the Rudbār area in the Sefidrud gorge, to the south of the coseismic surface rupture (Fig. 5). The 1991 November 28 source parameters may, therefore, be associated with the terminations of the Kabateh and Zardgeli strike-slip segments in the Sefidrud gap area.

(3) *Thrust Aftershocks at the Southern End of the Zardgeli Coseismic Strike-Slip Surface Rupture Segment:* Three aftershocks, which took place on 1990 June 21 at 05:35 GMT, M_s 4.6 (Gao & Wallace 1995); 09:02 GMT, M_w 5.6 with N–S thrust mechanism (Choy & Zednik 1997; Jackson *et al.* 2002), and at 13:46 GMT on the 2002 April 19, M_s 4.6, with N–S CMT solution (HRVD) are located near the southeastern terminus of the coseismic surface fault (Table 3, Figs 5 and 6). The largest aftershock of 1990 June 21 M_w 5.6 (09:02 GMT), with N–S reverse faulting mechanism at the southeastern end of the Rudbār left-lateral fault, took place about 12 hr after the mainshock. The 2002 April 19 (13:46 GMT, M_w 5.2) aftershock has the highest recorded peak ground acceleration of 166 cm s^{-2} (http://www.bhrc.ac.ir) at the Jirandeh accelerogram (36.70°N–49.78°E) located to the southeastern terminus of the coseismic surface rupture (Fig. 5); while the Sefidrud Dam-1 accelerogram, sited at 36.75°N–49.38°E, 37 km to the west of Jirandeh recorded a peak ground acceleration of 29.15 cm s^{-2}. Accelerations are consistent with a location closer to Jirandeh than to the Sefidrud dam.

Berberian *et al.* (1992), followed by Gao & Wallace (1995), proposed that due to the left-lateral strike-slip displacement along the Rudbār earthquake fault, the eastern portion of the Manjil thrust, where it bends to trend northeastward, was critically stressed and reactivated during the 1990 June 21 (09:02 GMT) M_w 5.6 aftershock. It is plausible that other cross-faults, such as the E. Darehtut fault, located further to the east of the Manjil thrust-bend were responsible for this aftershock (Fig. 4). The rationale behind this thought is that the 'exposed' segment of the northward-trending part of the Manjil thrust is very short and does not seem to be capable of creating an M_w 5.6 aftershock. *P*/*SH* body waveform modelling of the 1990 June 21 aftershock (Jackson *et al.* 2002) yields a nearly N–S thrust

Table 3. Source parameters of the 1990 June 20 Rudbār aftershocks (Fig. 6).

No.	Date	Origin time	Epicentre (N°–E°)	M_w	M_s	Strike (°)	Dip (°)	Rake (°)	Slip vector (°)	Centroid depth (km)	M_o (Nm)	Fault mech.	Method used	Source
1	1990 June 21	02:08	36.79–49.83[a]		5.4	291	80	-10	112	12	0.92×10^{17}	LLSS	SSMT/JMT	Gao & Wallace (1995)
2	1990 June 21	05:35	36.77–49.91[a]		4.6	302	50	54	78	6		T	SCD	Gao & Wallace (1995)
3	1990 June 21	07:50	36.87–49.52[a]		4.9	103	81	10	102	8		LLSS	SCD	Gao & Wallace (1995)
4	1990 June 21	09:02	36.65–49.83[a]	5.8	5.3	026	69	87		17	5.1×10^{17}	T	SSMT/JMT	Berberian *et al.* (1992)
				5.7							3.9×10^{17}	T	MedNet CMT	Giardini *et al.* (1994)
					5.8	23	64	92	105	8	4.0×10^{17}	T	SSMT/JMT	Gao & Wallace (1995)
				5.8		205	26	90	90	10	4.9×10^{17}	T	P waveforms	Choy & Zednik (1997)
				5.6		1	62	95	80	10	2.9×10^{17}	T	P/SH waveforms	Jackson *et al.* (2002)
5	1990 June 21	12:17	36.99–49.48[a]		5.3	302	51	54	85	6	0.8×10^{17}	T	SSMT	Gao & Wallace (1995)
6	1990 June 21	21:27	36.68–49.75[a]		4.9	103	81	10	103	8	1.1×10^{17}	LLSS	SSMT	Gao & Wallace (1995)
7	1990 June 21	21:31	36.85–49.43[a]		4.8	103	81	10	101	8		LLSS	SCD	Gao & Wallace (1995)
8	1990 June 22	06:07	37.25–48.90[a]		4.6	302	50	54	80	6	1.0×10^{17}	T	SSMT	Gao & Wallace (1995)
9	1990 June 22	06:21	36.87–49.53[a]		4.9	309	47	65	82	10		T	SCD	Gao & Wallace (1995)
10	1990 June 24	09:45	36.89–49.44[a]	5.5	4.8	235	70	−164		8	2.2×10^{17}	LLSS	SSMT	Berberian *et al.* (1992)
				5.3							1.1×10^{17}	T	MedNet CMT	Giardini *et al.* (1994)
					5.1	309	47	65	78	10	1.2×10^{17}	T	SSMT	Gao & Wallace (1995)
11	1990 June 24	19:05	37.00–49.53[a]		4.8	302	51	54	82	6		T	SCD	Gao & Wallace (1995)
12	1991 November 28	17:19	36.86–49.58[b]	5.7	5.0	350	47	80	95	8	3.89×10^{17}	T	P/SH waveforms	Jackson *et al.* (2002)
13	2002 April 19	13:46	36.67–49.74	5.2	4.6	183	26	103	79	18	7.75×10^{16}	T	CMT	HRVD
			36.56–49.81	5.2		1	47	94	86	18	7.06×10^{16}	T	CMT	ZUR-RMT

Notes: JMT: joint moment tensor inversion. LLSS: left-lateral strike-slip. SCD: simple comparison determination. SSMT: single station moment tensor inversion. T: thrust/reverse.
[a]Gao & Wallace (1995).
[b]ISC.

auxiliary nodal plane dipping E and a WNW–ENE plane dipping WSW consistent with the trend and geometry of the E. Darehtut fault (Figs 4 and 6). Some reverse NNW–SSE trending faults, including the E. Darehtut fault, are located in the compressional fault 'stepover' area between the southeastern extremity of the left-lateral Rudbār fault in the NW and the western segment of the Shāhrud thrust in the south; dipping S and WSW, rather than to the north as suggested by Tatar & Hatzfeld (2009) (Fig. 4). Apparently, the earthquake on the Rudbār fault caused strain transfer through the ∼13 km-width Rudbār-Shāhrud compressional fault stepover and reactivated the oblique faults between them. The Rudbār and the E. Darehtut fault system need to be considered as a single system for developing rupture scenarios for seismic hazard assessments.

3.3.2 Locally recorded aftershocks

Tsukuda *et al*. (1991) locally recorded aftershocks utilizing six portable seismographs during 1990 July 21 to 1990 December 11. While individual location errors are sometimes large, the data set taken as a whole indicates seismicity follows a narrow zone about 90 km striking N120°E with most activity concentrated along the southeastern end of the fault.

Eslāmi (1992) reported the distribution of all the aftershocks recorded by the Institute of Geophysics, Tehran University for the period of three months following the mainshock. Quality assurance analyses as well as a parametric list of the aftershocks were not provided. The scattered data show some correlation of the aftershocks with the coseismic surface faulting for the eastern segment, while the aftershocks located in the west are separated from the fault trace and shifted from it to the north. The author stated that the coseismic fault has a northeast high-angle dip. The majority of the aftershocks were concentrated between the surface and 15 km depth with the highest concentrations at 14 km depth. Nonetheless, in his cross section, the foci continue down to 60 km depth. Eslāmi (1992) also claims that towards the northwest the number of the aftershocks diminishes while their focal depths increase. Due to lack of quality assurance analysis in the article, the conclusions stated by the author cannot be verified.

Hamzehloo *et al*. (1997a) reported master event relocations of 36 aftershocks originally recorded by five local stations during 1990 July 5–22 using only *P* arrivals by the Institute of Geophysics, Tehrān University (Rezāpour 1991). The relocated aftershocks defined a narrow belt oriented N125°E, with focal depths ranging from 1 to 16 km depth. To the southeast, the aftershocks are shifted to the NE from the Zardgeli segment of the surface rupture, but to the west, some aftershocks were located near the Kabateh segment.

3.4 Microearthquake survey

About eight years after the Rudbār earthquake a microearthquake survey utilizing 30 portable seismographs was deployed along the fault and recorded 410 events (Tatar 2001; Tatar & Hatzfeld 2009). The seismicity included 276 events with locations constrained by at least eight *P* and *S* arrivals, rms residuals <0.12 s, horizontal and vertical uncertainties <1 km, and azimuthal gap <180°. The microseismicity forms a wide zone of seismic activity trending NW–SE. As with the aftershock sequence, the blurred microearthquake activity of 1998 was clustered in: (i) the Sefidrud coseismic surface fault gap area and (ii) the southeastern termination of the 1990 surface rupture near Jirandeh (Figs 4 and 5). The majority of focal depths ranged from 8 to 16 km (Tatar & Hatzfeld 2009). Very little activity was recorded along the Kabateh segment west of the Sefidrud gorge, and almost no activity was recorded along the northwestern termination of the fault. The Baklor and the western half of the Kabateh segments, were not covered by any station.

Tatar & Hatzfeld (2009) interpret the microseismicity as indicating an overall partitioning of slip onto parallel strike-slip and northward-dipping thrust segments. In particular, they suggest that many of the epicentres adjacent to the eastern, Zardgeli, segment of the 1990 rupture indicate activity on a reverse fault, dipping northward at ∼45°, and projecting the surface close to, but with an opposite dip direction to, the Shāhrud thrust (e.g. Fig. 4). It seems that, just as microearthquakes are clustered around the Sefidrud coseismic gap, the cluster of microearthquakes at the southeastern end of the 1990 ruptures may indicate the structural boundary between the Rudbār and the Kashachāl faults to the north, and the activity of the E. Darehtut region to the south (see Fig. 4 and Sections 5.1 and 5.2). Comments on the dip of the coseismic surface rupture are already addressed in the aftershock section above (Section 3.3.1a).

4 COSEISMIC SURFACE FAULTING

Different field interpretations and many speculative coseismic fault maps have been provided by several incompatible field reports, which caused confusion in almost all the published reports since 1990. It is, therefore, necessary to comment on the misreported coseismic surface ruptures entered in the literature.

Moinfar & Nāderzādeh (1990) reported 85 km of coseismic right-lateral surface faulting with a straight trend of N112°E, partly along the Manjil thrust (Berberian & Qorashi 1984; Berberian *et al.* 1992). Their coseismic surface fault passes at about 300 m north of the Sefidrud dam, allegedly showing 20 cm right-lateral and 50 cm vertical displacements. Their proposed coseismic fault, which misidentified landsliding as surface rupture, is located 12.5 km to the south of the coseismic surface rupture of the 1990 earthquake in the west, and 10 km to the south along the Sefidrud River. They also mapped a questionable fault trace of 12 km long, striking N152°E in the area of Baklor to the NW. The location and the reported mechanism for this fault, can neither be supported by the mainshock long-period *P* and *SH* body wave inversions (Thio *et al.* 1990; Gao *et al.* 1991; Berberian *et al.* 1992; Gao 1993; Campos *et al.* 1994; Giardini *et al.* 1994; Gao & Wallace 1995), nor by the field observation (Fig. 4).

Dashti (1990) introduced several major longitudinal and transverse active faults in a crisscross pattern, which presumably moved during the earthquake. No evidence of such a 'chicken-fence' pattern surface faulting was observed in the field study carried out immediately after the earthquake.

Pursuant to Moinfar & Nāderzādeh (1990), Zāre' (1991a,b) and Zāre' & Moinfar (1993, 1994) followed by Māheri (1991), Niāzi & Bozorgniā (1992), Haghshénās (1998) and many others, introduced two coseismic surface faults for the 1990 earthquake. (i) The '*Harzevil fault*' along the Sefidrud dam axis (the Manjil thrust of Berberian & Qorashi 1984; Berberian *et al.* 1992; see Figs 4 and 5 for the locations) with no data of the length or amount of displacements; and (ii) the '*earthquake fault of the Sefid Rud Dam*' with 3 km length and 10–70 cm displacement (Zāre' 1991a) or 5 km with 0.3 m left lateral and 0.5 m upward movement of the northern part at the left abutment hill top of the Sefidrud Dam (Zāre' 1991b). The latter was considered as 'the most important earthquake fault that is associated with the main event'. Some evidence of disturbance were noticed along portions of the Manjil thrust front during the earthquake, but as reported by Berberian *et al.* (1992) the disturbances

were associated with slope failure and not related to the fault reactivation with thrust and or strike-slip mechanism. Coseismic motion of the fault at the highway Tunnel near the Sefidrud dam and Harzehvil (east of the Dam) is also mentioned by Ramazi (1991), which in fact was caused by landslides. Note that the locally recorded aftershocks conducted immediately after the earthquake (Rezāpoor 1991; Tsukuda *et al.* 1991; Eslāmi 1992; Hamzehloo *et al.* 1997a), and the microearthquake survey (Tatar & Hatzfeld 2009), discussed earlier, do not support any seismic activity along the Manjil (Harzehvil) thrust. They also do not support the so-called 'earthquake fault of the Sefid Rud Dam' in this area during the mainshock. See Figs 4 and 5 for geographic locations.

Ramazi (1991) correctly reported 15 km of the eastern, Zardgeli, segment of the faulting with maximum left-lateral displacement of 100 cm and vertical displacement of 50 cm. In their later publication, Zāre' & Moinfar (1993, 1994) and Zāre' (1995) speculated 'six coseismic faults' distributed to the north and the south, and collectively called them the 'Earthquake Origin Zone'. Their 'southern coseismic faults' were the Harzehvil, the Sefid-Rud Dam [5 km long, 30 cm left-lateral slip, 50 cm reverse slip, with N110°E strike], the Borehbon [sic., Barehbon; 16 km, N102°E], and the Pākdeh [1.5 km, N128°E; see below] faults. Whereas their 'northern coseismic faults' included the Baklor [3 km long, 40 cm left-lateral displacement, N-S trend], the Āb-Bar [2.5 km, N127°E], and the Kabateh [5 km, N130°E] faults (Zāre' & Moinfar 1993, 1994).

Ishihara *et al.* (1992) combined the speculated 'northern' and the 'southern' faults together and introduced a single arcuate ground rupture of 100 km long. It extends from Baklor in the NW to Guilévān in the south with a strike of N150°E, and then curving to almost E-W direction from Guilévān to the Manjil Dam and then to Pākdeh in the east (see Figs 4 and 5 for the locations). Ishihara *et al.* (1992) reported maximum horizontal and vertical coseismic displacements of 20 and 50 cm, respectively. Finally, Hamzehloo *et al.* (1997b) suggested that the 1990 Rudbār earthquake was caused by the Sefidrud Dam impoundment.

Except for Berberian *et al.* (1992), none of the above-referenced publications referred to the important issue of the coseismic surface rupture gap at the Sefidrud gorge. Moinfar & Nāderzādeh (1990), Zāre' (1991a,b), Ramazi (1991), Māheri (1991), Ishihara *et al.* (1992) and Skovorodkin *et al.* (1999) are amongst others who draw their speculative coseismic surface ruptures cutting the Sefidrud gorge and the highway passing through at different locations from the dam-site to the north.

The 80 km coseismic range-parallel left-lateral strike-slip faulting of the 1990 earthquake occurred on a fault that was previously unknown, and was not mapped on the 1:250 000 geological maps of the area published prior to the event (Stocklin & Eftekhārnezhād 1969; Annells *et al.* 1985a,b). The western portion of the fault, sited west of the Sefidrud deep gorge, was also not shown on the 1:100 000-scale post-earthquake geological map of the area (Nazari & Salāmati 1998), while only about 15 km of the eastern end of the fault is marked on the neighbouring map (Ghalamghāsh & Rashid 2002).

The fault has a subtle expression in the pre-1990 earthquake geomorphology, and only in a few places, it is clearly recognizable on aerial photographs and satellite imagery amongst numerous thrusts and nappes of the 'High-Alborz' (Figs 4, 8a, and b). Apparently, the fault does not move often enough to exert much influence on the topography. Near Jayshābād along the western segment of the earthquake fault (36.85°N–49.15°E; Fig. 5, also see Fig. 11), an older fault escarpment with an approximate height of 6–10 m is exposed on the southern Late Jurassic–Early Cretaceous limestone block elevated against the northern downthrown Eocene volcanic rocks (Figs 8a and b). This is one of the clearest locations along the Rudbār fault where the fault trace is visible on aerial photographs and satellite imagery. The 1990 vertical motion at this locality was 120 cm. At this locality, the Kabateh fault segment had a nearly vertical dip with slight inclinations towards the SSW (Fig. 8b). To the southeast, the Zardgeli segment shows some reverse slip dipping to the SSW (Figs 9a and b).

Assuming a fault length of 80 km, the depth of 15 km, and the rigidity of 3×10^{10} Nm^{-2}, the calculated seismic moment is able to account for an average seismologically determined slip of 240 cm, which is much more than the observed displacements in the field (Fig. 5). This discrepancy could be due to some factors such as: (i) the fault and the displacements were not thoroughly mapped immediately after the earthquake; (ii) the rupture might have propagated deeper than 15 km, though the microseismicity data of Tatar & Hatzfeld (2009), suggest that the majority of seismic deformation is limited to $<$16 km depth; and (iii) not all the slip reached the surface. Note that, for instance, the 1992 June 28 Landers, CA. Earthquake, which was of similar magnitude of M_w 7.3 and produced the same amount of 80 km surface rupture, with an 8 km source depth, accommodated 6 m right-lateral and 2.5 km vertical motion (Arrowsmith & Rhodes 1994; Johnson *et al.* 1994).

The striking features of the surface ruptures of this earthquake (Fig. 5) were that:

(i) The 1990 coseismic surface rupture was composed of three main right-stepping en-échelon left-lateral strike-slip fault segments of the Baklor, Kabateh (west of the Sefidrud gorge gap) and Zardgeli (east of the surface gap) with nearly vertical dip. No single fault segment extended more than half of the total length of the system (Fig. 5).

(ii) The coseismic surface fault did not cross the Sefidrud deep gorge, its elevated Quaternary terraces, or the highway running along the River (Fig. 5), and no surface deformation was observed during the mainshock and/or the aftershock activities in the gorge. The Sefid Rud may, therefore, be located at an important discontinuity in the fault.

(iii) The surface rupture virtually followed the drainage divide of the 'High-Alborz' very close to the peak of the western 'High-Alborz', and mostly at or above elevation +2000 m (Fig. 5).

(iv) The coseismic vertical displacements along the total length of the earthquake fault were consistently down to the north and northeast, in the opposite sense to the existing topography (Figs 7b–c, 8a–c and 9). For example, the ridge of the 'High-Alborz' located immediately to the NNE of the coseismic fault at Jayshābād, with two peaks at elevations +2867 m and +2776 m (Fig. 5), dropped down by one meter (opposite to the existing topography) during the 1990 earthquake. The coseismic faulting thus had a tendency to reverse the existing topography of the 'High-Alborz' Mountains.

(v) A large portion of the strike-slip deformation occurred in a narrow zone of about 6–10 m wide.

(vi) The amount of vertical displacement was usually more than the amount of the left-lateral displacement in the locations visited (Fig. 5).

(vii) In addition to main left-lateral slip, the western fault segments, the Baklor segment as well as the western portion of the Kabateh segment, showed local surface evidence of slight normal-slip component in the form of large open fissures (Fig. 7). In contrast the eastern segment of the Kabateh and the most of the Zardgeli segments were associated with slight reverse-slip component in the form of push-ups (Figs 8a,b, 9a and b).

(viii) The fault plane was nearly vertical with slight dip towards the SSW (Figs 7b–c and 8a,b).

(ix) The subtle topographic expression of the Rudbār fault suggests that the fault does not move often enough to exert much influence on the geomorphology of the soft rocks.

The northwestern Baklor segment, situated ∼2.5 km south of Baklor village (Fig. 5) is the shortest segment of approximately 10 km length, and showed the least left-lateral (5 cm) and vertical (15 cm) displacements (Fig. 7a) along the whole surface rupture of 80 km long (Fig. 5). A minor displacement along a fault passing immediately north of Baklor was also documented immediately after the earthquake. However, the displacements diminished and died out towards the end of the segments. Site visits 10 yr after the earthquake showed that the minor surface slips were washed out by erosion. The mainshock was also associated with bedding plane slip with thrust mechanism showing coseismic folding in High-Alborz (Berberian *et al.* 1992).

4.1 Pre-1990 seismicity of moderate-sized pure thrust earthquakes and possible loading of the 1990 large-magnitude strike-slip earthquake

The narrow active belt of the Alborz Mountains is pervaded by a high-density of intersecting range parallel thrust and strike-slip faults. In this complex situation with parallel faults of approximately equal length and possibly of equal strength, the state of stress on one fault becomes dependent on the state of the stress of the adjacent fault and elastic interactions between the elements of the system. When a section of this narrow belt—such as the Rudbār area in the western High-Alborz—becomes critically loaded, the failure of a thrust fault may result in stress redistribution that critically loads the adjacent strike-slip or another thrust fault. The 1990 June 20 (M_w 7.3) Rudbār earthquake was preceded by at least four medium-magnitude earthquakes in the region during the 20th century (Table 4).

The 1983 July 22 (M_w 5.4) Charazeh earthquakes (Fig. 4) involved high-angle reverse faulting dipping 55° northeast (Priestley *et al*. 1994) probably on the Manjil thrust, and its macroseismic epicentre of 36.90°N–49.19°E (Berberian *et al.* 1992) is in the general area of the initial rupturing point of the 1990 June 20 M_w 7.3 strike-slip event (Fig. 5). It is possible that the 1983 earthquake with pure thrust mechanism on the Manjil thrust interacted with the Rudbār strike-slip fault at depth and had a loading and triggering effect on it.

4.2 Intersection of the Manjil thrust and the Rudbār strike-slip fault within the seismogenic layer

The proximity in space and time of the Manjil thrust and the Rudbār strike-slip fault (Figs 4 and 5) and the seismic activity during the 20th century (Table 4) suggest that these faults may interact with each other at depth. The Manjil Thrust was probably reactivated during the 1983 July 22 M_w 5.4 Charazeh earthquake (Fig. 5). Given the source parameters of the 1983 event (strike 308°; dip 55°NE; rake 94°; centroid depth 10 km; slip vector 30°; moment 1.88×10^{17} Nm; Priestley *et al.* 1994) the Manjil thrust would eventually intersect the vertical Rudbār left-lateral strike-slip fault within the seismogenic layer of ∼16 km (Berberian *et al.* 1992; Berberian 1997).

Table 4. Pre-1990 June 20 (M_w 7.3 Rudbār earthquake) regional seismicity of moderate-sized earthquakes.

Earthquake date	Time (GMT)	Macroseismic epicentre (N°–E°)	M	m_b	M_s	M_w	I_o	Region	Causative fault
1903 June 24	16:56				5.9		VII+	Ānzali	
1905 January 09	06:17	37.08–48.18			6.2		VIII	Darrām	Manjil Thrust
1924 November 08	09:05		5.5						
1948 June 17	14:08	36.70–49.15	5.5				VII+	Āltinkosh	
1948 June 30	19:31		5.0				VI+	Āltinkosh aft.	
1956 April 12	22:35		5.5				VII	Langerud	
1968 August 02	03:59	36.75–49.38		4.7			VI	Sefidrud Dam	Manjil Thrust
1970 January 19	17:19			4.6	4.0		V	Rudbār-Tārom	
1978 November 04	15:22	37.65–48.95		6.1	6.0		VII+	Siāhbill	Āstārā Thrust
1980 January 13	05:51			5.0	4.8		VI	Rudsar	Khazar Thrust
1980 May 04	18:35	38.10–48.80		5.4	5.4	6.3	VII	Shirābād	Āstārā Thrust
1980 July 22	05:17			5.3	5.1		VI+	Lāhijān	Khazar Thrust
1980 August 27	20:11			4.1			V	Tārom	
1980 December 03	04:26			5.1	4.7		VI	Rudsar	Khazar Thrust
1983 July 22	02:41	36.87–49.19		5.6	5.0	5.45	VII	Charazeh	Manjil Thrust
1983 July 23	08:05			4.4	4.2		VI+	Charazeh Aft.	Manjil Thrust
1983 December 20	22:21			4.8			VI	SW Tonékābon	Khazar Thrust
1983 December 21	00:07			4.3			V+	SW Tonékābon	Khazar Thrust
1984 March 18	16:56			4.2			V+		Āstārā Thrust
1984 September 30	15:32			4.6			VI	Hashtpar	Āstārā Thrust
1985 February 20	19:59			4.3					Āstārā Thrust
1986 September 10	19:32			4.2					
1988 January 14	11:29			4.4					
1989 February 15	10:10			4.7	5.0		VI+	Rudbār	
1989 October 08	14:13			4.6			VI	Rasht	
1990 April 20	13:05							Rudbār-Tārom [Rudbār Foreshock]	
1990 June 20	21:00			6.2	7.4	7.3	IX^+	Rudbār-Tārom [Rudbār Mainshock]	Rudbār LLSS

Notes: Aft: aftershock. LLSS: left-lateral strike-slip fault. M: unidentified magnitude.
[a]Priestley *et al.* (1994).
[b]See Table 2.

4.3 Slip partitioning in the high-Alborz

The compressional axes and slip vectors inferred from the focal mechanisms in the Alborz are consistently directed NE, implying a small component of left-lateral motion across the Alborz (Jackson & McKenzie 1984). The 1990 Rudbār earthquake provided evidence that the High-Alborz is also undergoing left-lateral slip (Berberian *et al.* 1992). Slip vectors of the 1990 Rudbār mainshock and the strike-slip aftershocks are perpendicular to the general direction of the nearly NE–SW shortening in the High-Alborz, whereas most adjacent thrust earthquake and aftershock slip vectors are in the general NE–SW regional convergence (Berberian *et al.* 1992; Gao & Wallace 1995; Berberian 1997; Choy & Zednik 1997; Jackson *et al.* 2002). A similar case is observed between the 1983 July 22 M_w 5.4 Charazeh earthquake with high-angle reverse faulting (slip vector N30°E) and the 1990 June 20 Rudbār strike-slip main shock (slip vector N120°E) with overlapping meizoseismal regions (Berberian *et al.* 1992; Priestley *et al.* 1994; Jackson *et al.* 2002; Fig. 5). The approximately 82° difference in slip vectors indicates that the oblique regional conversion between the Alborz and the South Caspian block is partitioned into pure left-lateral strike-slip and pure thrusting in the western High-Alborz, where strains are large, and where high topography and intense folding and faulting has occurred. Slip partitioning into pure shortening and pure strike-slip is a way in which the faults can take up large finite strains (McKenzie & Jackson 1983; Jackson & McKenzie 1985, 1988; Priestley *et al.* 1994; Jackson *et al*. 2002).

5 ACTIVE FAULT GEOMORPHOLOGY OF THE RUDBĀR REGION

One of the most surprising and potentially worrying aspects of the 1990 Rudbār earthquake is the extremely subtle expression of the fault in the geomorphology. The Rudbār fault was not identified prior to the 1990 earthquake and it is possible that additional unmapped active faults are present within the Alborz Mountains.

The subtle morphology and lack of obvious cumulative displacement is in contrast to range-parallel strike-slip faults further to the east in the Alborz, which are clearly visible on satellite imagery, and have cumulative displacements of up to 35 km (Jackson *et al.* 2002; Allen *et al*. 2003; Hollingsworth *et al.* 2006). Jackson *et al*. (2002) conclude that the rates and total cumulative slip of range-parallel left-lateral strike-slip in the western part of the Alborz are lower than those in the east. They relate the apparent change in rate to the motion of the South Caspian block relative to Iran.

In the following discussion we assess, using SRTM digital topography (Shuttle Radar Topography Mission; Farr & Kobrick 2000), and ASTER satellite imagery the indications of cumulative slip in the Rudbār region. The 1990 event is not the first recorded destructive earthquake in the western Alborz. The faults we describe are possible sources of the Upper Polrud earthquake in 1485 A.D. and the 1608 A.D. Alamutrud earthquake (described in Section 6), both of which define regions of intensity IX similar in area to that of the 1990 Rudbār earthquake (Fig. 7a).

5.1 Rudbār fault

Fig. 10 shows the 1990 Rudbār earthquake ruptures, marked in red, along with other major faults and major rivers of the western 'High-Alborz'. ASTER satellite imagery of the western part of the Rudbār fault, between the villages of Jayshābād and Namakrud, is shown in Fig. 11 with the part of the fault that ruptured in 1990 lying between the white arrows. Cumulative, up-to-the-south displacements, which have reversed the overall southward slope, are visible in the southeast corner of the image (Figs 8a and b; also see fig. 9b in Jackson *et al*. 2002). There is little in the way of cumulative left-lateral displacement of southwest-flowing rivers as they cross the fault. Possible left-lateral deflections of ∼1 km are noted for three rivers between 49°06'E and 49°10'E (Fig. 11). However, these apparent deflections are all downhill and may not be caused solely by cumulative fault movement. West of the section that ruptured in 1990, a series of three southward-flowing rivers show disruption of their otherwise rather linear courses, coincident with land-sliding of the steep valley sides (Fig. 11). The disruption to the river courses is consistent in each case with left-lateral deflection of the rivers by ∼1 km. However, as for the three examples described from near Jayshābād, whether the apparent deflections are caused by fault movement is not clear.

The topography of the eastern end of the 1990 ruptures (represented by red lines) is shown in Figs 12(a), 13(a) and (b). At this longitude, the Rudbār fault is only one of three east–west faults that appear to be active in the late Quaternary; the other two faults being the Kelishom fault and the Kashachāl fault (Figs 5 and 12a). The east–west trending Kashachāl fault appears to branch off the Rudbār fault close to its eastern end at Jirandeh (Figs 12a, 13a and b). There is little in the way of cumulative displacement along the eastern part of the Rudbār fault. A slight scarp and southeast-flowing stream following the trace of the ruptures are the clearest indicators of cumulative fault movement and none of the incised, southward-flowing streams is displaced as they cross the fault (Figs 10b, 13a and b). In contrast, the Kashachāl fault, which is situated ∼1 km north of the Rudbār fault at this longitude (Figs 4, 5 and 12a), shows very clear indications of both vertical and horizontal cumulative displacement (see Section 5.2).

5.2 Kashachāl fault

The south-facing scarp of the Kashachāl fault (Fig. 10a) is particularly clear in the western part of Figs 12 and 13 due to the abrupt break in incision south-flowing streams as they cross the fault. Five south-flowing incised streams show consistent and very clear, left-lateral displacements of 150–200 m. A sixth stream, labelled x in Fig. 13(b), shows an apparent right-lateral displacement. We argue however that stream x used to flow into a, now abandoned, channel on the southern side of the fault. At least 150–200 m of left-lateral displacement is thus demonstrated for the Kashachāl fault. Further east of Fig. 12(a) the Kashachāl fault tracks across the ridge of Aznā Chāk Mountain [lit., 'Fractured/Faulted Aznā'] reaching elevations of >3000 m at longitude ∼50°15′E. Both south-facing and north-facing scarps are present (e.g. Fig. 14a) indicating changes in dip direction along strike. The fault is often associated with a line of vegetation (red in the images, Fig. 14b) suggesting the presence of springs along the fault. Cumulative strike-slip displacements are not observed at any point apart from those shown in Fig. 13(b).

5.3 Kelishom fault

The third east–west fault within this western part of the 'High-Alborz' is the Kelishom fault (Figs 4, 12 and 15). This fault, which is located about 10 km to the NNE of the Rudbār fault, is mapped as a high-angle reverse fault dipping south (Berberian *et al.* 1983, 1992). However, we suggest it may be active in the late Quaternary with a left-lateral strike-slip component. The Kelishom fault, as

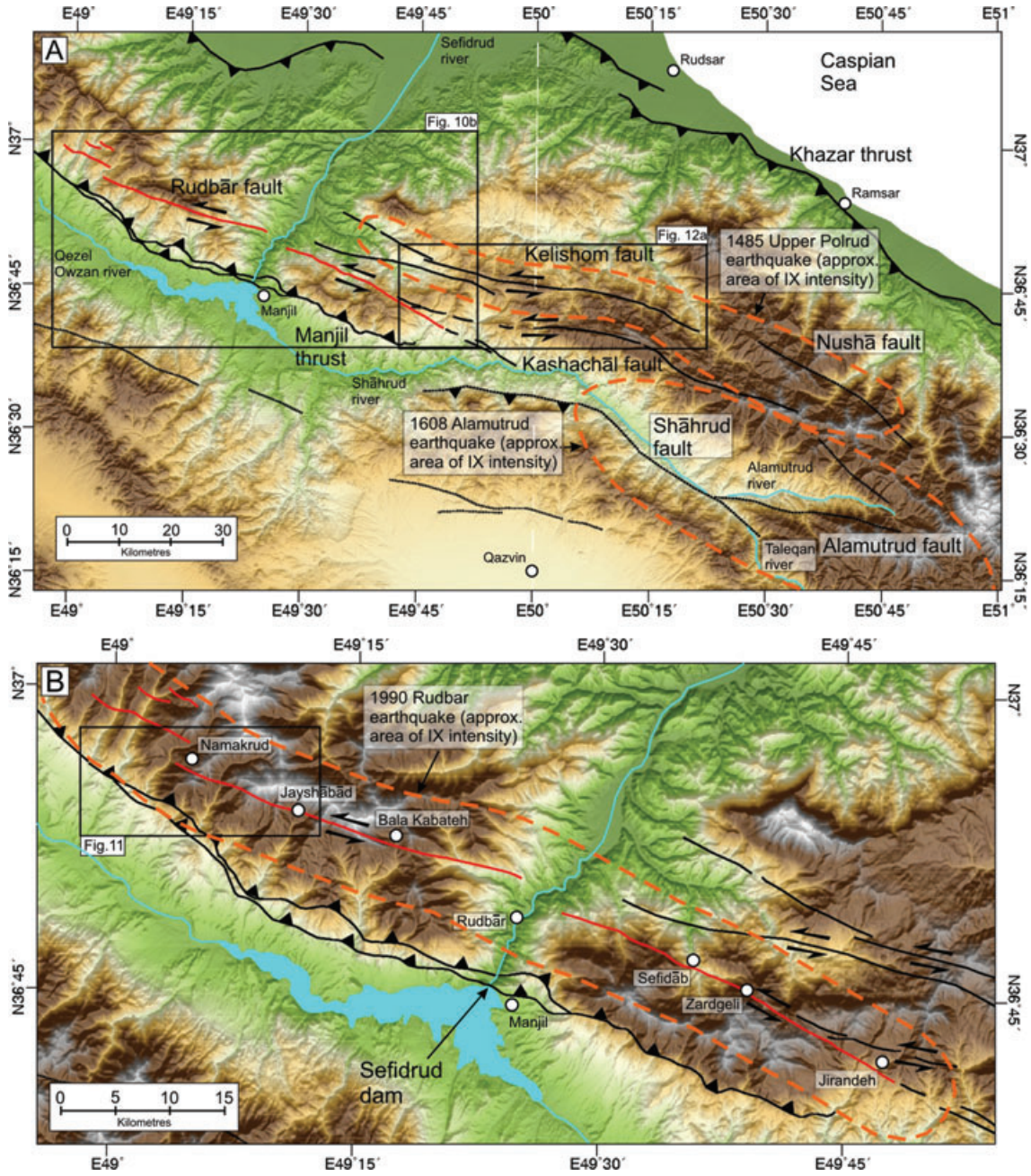

Figure 10. (a) Shaded-relief SRTM topography (Farr & Kobrick 2000) of the western Alborz with major faults and settlements referred to in the text. The red lines represent faults that ruptured in the 1990 Rudbār earthquake. Major rivers are drawn in blue. The Shāhrud River, with distinct northwest-flowing and west-flowing segments may be influenced by the orientation of the main faults. The orange dotted lines define the intensity IX isoseismals for the 1485 A.D. Upper Polrud and 1608 Alamutrud earthquakes. The Nushā, Shāhrud, and Alamutrud are unclear in satellite imagery and are instead mapped from aerial photographs and geological maps. (b) SRTM topography of the 1990 Rudbār earthquake region (see part 'a' for location). The orange dotted line defines the intensity IX isoseismal for the 1990 Rudbār earthquake (Fig. 5). Other ornamentation is as in part (a).

with the Rudbār fault, is approximately 90 km in length (Figs 10a and 12a, Table 5), and extends east from the Sefidrud gorge along the southern slopes of Dorfak Mountain (Figs 4 and 5). To the west, the Kelishom fault dies out near the Daylamān thrust, and like the Rudbār fault, it does not cut the Sefidrud gorge (Figs 4 and 5). To the east, in the upper Polrud River, the Kelishom fault splays out and is cut by the NW–SE trending right-lateral Nushā fault (Berberian *et al.* 1983). The Kelishom fault follows the southern slopes of the 'High-Alborz' approximately six km below the drainage divide at elevations of +2000 and +3000 m. To the east, the upper reaches of the Polrud River and its tributaries at elevations between +2000 m to +3000 m are influenced and directed by the eastern segment of the Kelishom fault and its splay branches. Huge areas of palaeo-rock avalanche, landslip, and rockfall in the epicentral region may in part be associated with active fault movements in the 'High-Alborz' along the Kelishom fault. We note, however, that field observations by J.-F. Ritz (personal communication 2008) did not find clear evidence of recent fault movements along the eastern segment of the Kelishom fault and it is possible that some of the scarps we identify may, instead, be erosional in origin.

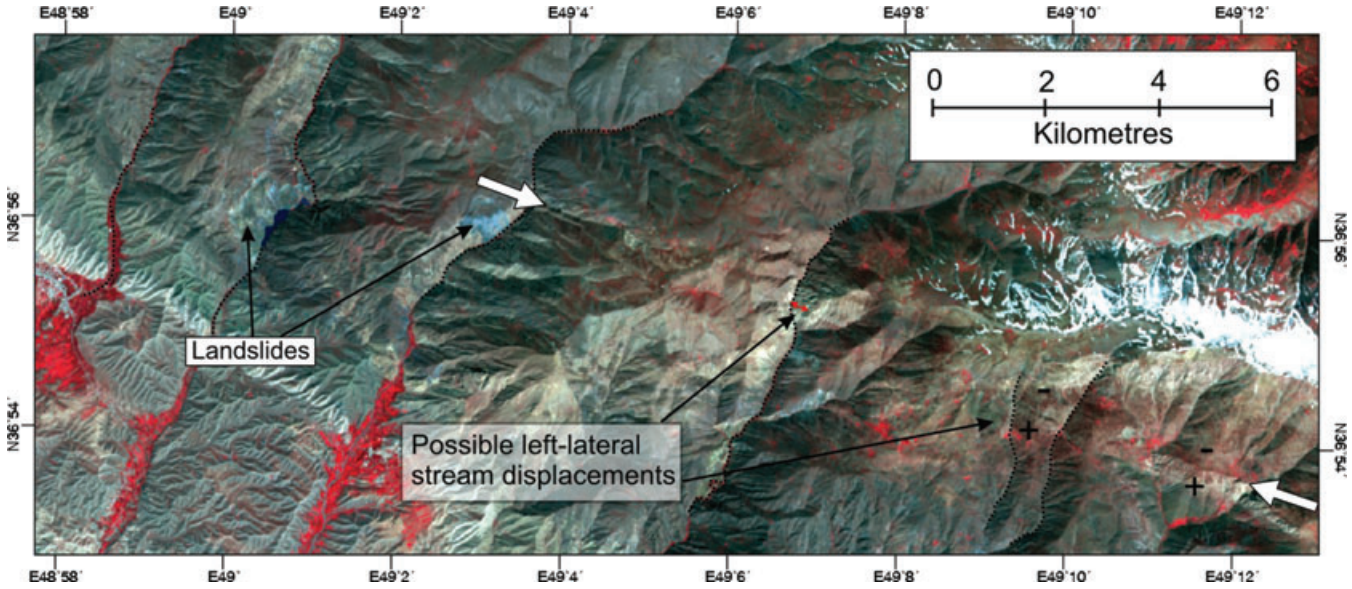

Figure 11. ASTER imagery (this, and all later ASTER images, use RGB 3n,2,1 such that vegetation appears red) of the western end of the 1990 rupture (between the white arrows; see Fig. 10b for location). The three rivers west of the end of the rupture show disruption (consistent with left-lateral displacement of ∼1 km) and land-sliding in an east-west alignment that might indicate that the fault continues further west than thought. The steep valleys and land-sliding may have helped to disguise river displacements. A clear cumulative scarp at the eastern end of the image (at ∼36°54′N 49°12′E) is featured in Fig. 9b of Jackson *et al*. (2002).

As with the Kashachāl fault, the facing-direction of the Kelishom fault scarp varies along strike (Figs 15a and b), suggesting changes in dip direction. The fault crosses several rivers that flow northward toward the Caspian Sea. Several of these rivers show apparent left-lateral displacements at the fault of between 0.4 and 1.5 km (Figs 12a and 15a; Table 5). Satellite imagery of several of these river displacements are shown in Fig. 15. In some cases, the drainage divide between adjacent northward-flowing rivers is also displaced laterally (Figs 15a and b), providing additional confidence in the drainage displacements being caused by cumulative fault movement. Not all the rivers, however, show drainage displacements. Two river systems along the easternmost 5–10 km of the fault show no displacement at all (Fig. 12a). We suggest that the eastern part of the Kelishom fault, where the trend changes from east–west to NW–SE, might have a larger component of shortening than the western sections. The fault runs through the meizoseismal area of the 1485 August 15 Upper Polrud earthquake and could have been reactivated during this event (see Section 6.1).

5.4 Alamutrud fault

The Alamutrud fault is located to the south of the Kashachāl fault and runs parallel to the southern edge of the E–W trending Alamutrud valley (Fig. 10a). To the northwest it splays off the Shāhrud fault, which itself parallels the southern edge of the Shāhrud valley (Figs 4 and 10a). The fault system, with a total length of > 75 km, has created a major topographic feature along which the major Shāhrud and Alamutrud Rivers flow from elevations of about +3000 m in the east to about +1000 m in the west. It is a reverse fault dipping south along which the southern Eocene volcanic rocks (the Karaj Formation) are thrust over the northern Neogene molasse deposits. The highly sheared zone of the fault, with fresh slickensides, trending N130°E plunging 20°NW, is visible along the Qazvin-Mo'alem Kalāyeh road (figs 4.24 and 4.25 in Berberian *et al.* 1983). Numerous landslides are visible along the fault trace. During the 1945 September 27 earthquake (VII) half of Heriān village located on the Alamutrud fault [36.43°N–50.30°E] was destroyed and three other villages including Hasanābād located in the northern vicinity of the fault were damaged (Berberian *et al.* 1983). The fault runs through the meizoseismal area of the 1608 April 20 earthquake and could have been reactivated during this event (see Section 6.2).

5.5 Nushā fault

The Nushā fault is a NW–SE trending fault with a length of about 57 km located at the eastern end of the Kelishom fault, in the area NW of the Alamkuh (Annells *et al.* 1985a,b; Berberian *et al.* 1983). It is composed of several parallel fault strands starting from the NW–SE section of the Polrud River in the northwest to the Alamkuh granite at elevation of 3000 m in the southeast. The fault offsets the 98 Ma Nushā pluton right-laterally for about 13 km (Guest *et al.* 2006). Geomorphic features showing lateral displacement are not observed in satellite imagery. The present-day activity of the Nushā fault cannot, therefore, be assessed through remote sensing. It is possible that the Nushā fault has not been reactivated during the most recent history of the western 'High-Alborz' in which deformation in the high parts of the range is dominated by left-lateral strike-slip faulting (e.g. Jackson *et al*. 2002; Allen *et al*. 2003; Ritz *et al*. 2006).

5.6 Summary of active faults

In summary, west of the Sefidrud deep gorge, the 1990 Rudbār earthquake fault is the only recently mapped strike-slip fault and may show cumulative left-lateral displacements of up to ∼1 km. East of the Sefidrud gorge, the active faulting is more complex, and we show that the fault that broke in the 1990 Rudbār earthquake is only one of up to three parallel faults showing indications of late Quaternary activity. The eastern part of the Rudbār fault shows little evidence for cumulative left-lateral motion. Of the other two faults, the Kashachāl fault shows clear evidence for ∼150–200 m of left-lateral displacement. The Kelishom fault shows a series of apparent

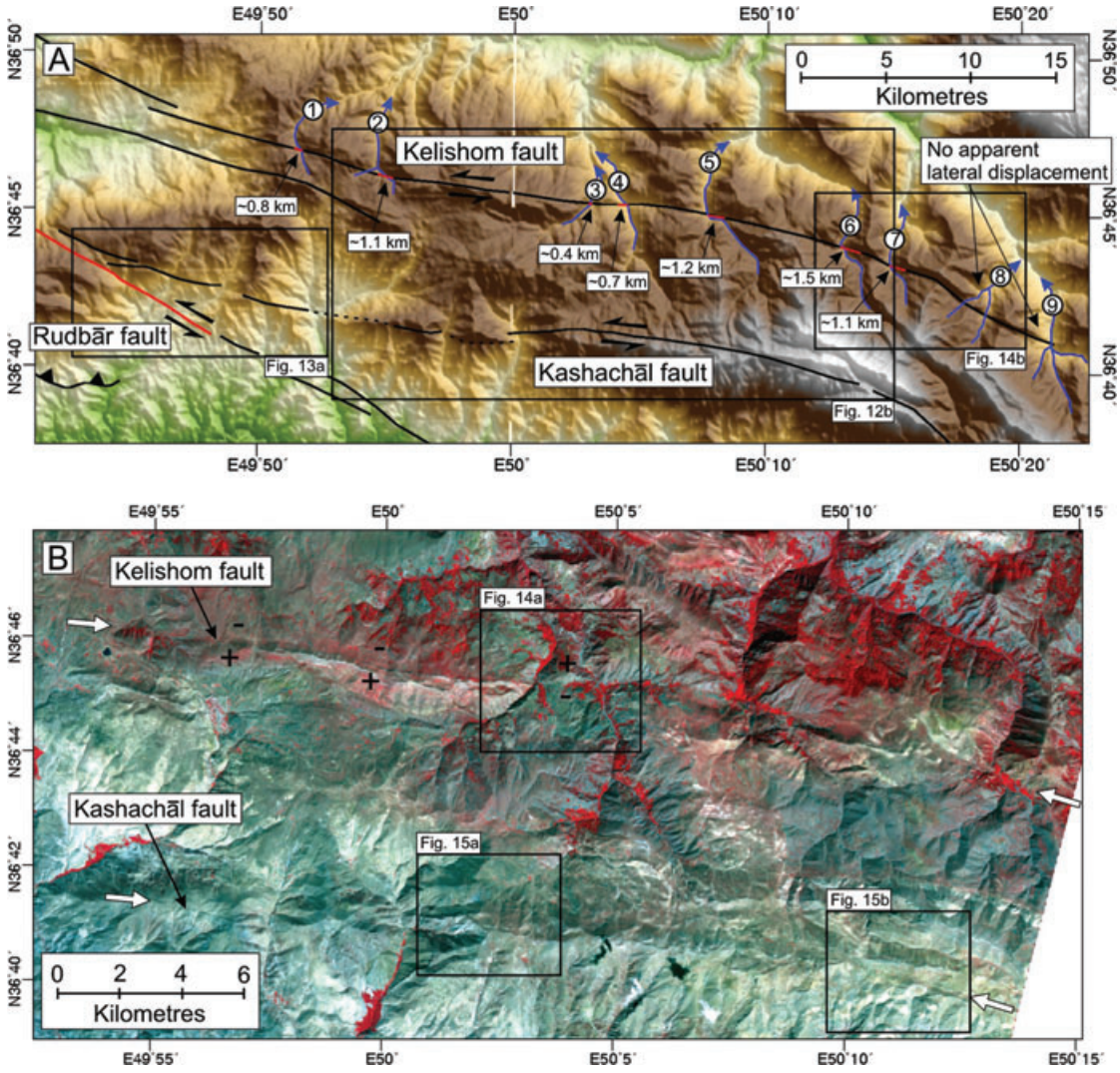

Figure 12. (a) Shaded-relief SRTM topography of the Kelishom and Kashachāl faults at the east end of the 1990 Rudbār rupture (marked in red). Northward-flowing rivers that cross the Kelishom fault appear to be displaced left-laterally by amounts between 0.4 km and 1.5 km (displacements marked by red lines). For the numbers see Table 5. See Fig. 10a for location. (b) ASTER imagery of the Kelishom and Kashachāl faults (see part 'a' for location). Both faults show clear scarps that change in polarity along strike. '+' and '−' symbols denote the uplifted and down-dropped sides of the fault at those points. See later Figures for detailed views of the fault scarps.

left-lateral river displacements between 0.4 km and 1.5 km (though there is discussion as to whether the eastern Kelishom scarps and river displacements are fault-related or erosional in origin; J-F. Ritz, personal communication, 2008). Summed together, the three faults are unlikely to have accommodated more than 2 km of cumulative left-lateral slip.

6 HISTORICAL (PRE-1900) SEISMICITY OF THE RUDBĀR REGION

6.1 The 1485 August 15 upper polrud earthquake [$I_o \sim$ IX, $M_s \sim 7.2$]

The 1485 large-magnitude earthquake was experienced by Mar'ashi (1489) and the ruler of Daylamān (see Figs 4 and 5 for the location), Soltān Mirzā 'Ali. The latter was at prayers when the buildings at Daylamān collapsed but he was able to escape the disaster (Mar'ashi 1489; Rabino 1928; Sotudeh 1968; Nabavi 1972; Ambraseys 1974; Ambraseys and Melville 1982; Berberian *et al.* 1983, 1992; Berberian 1994). Ambraseys and Melville (1982) estimated an equivalent surface wave magnitude of 7.2 for this event. The earthquake caused a widespread destruction and damage in eastern Guilān and western Mazandarān provinces of northern Iran, in the 'High-Alborz' Mountains south of the Caspian Sea.

Summary of the macroseismic data reported by Mar'ashi (1489), who was sent to the upper Chālakrud [Chālak River] Gorjiān district, is set forth in Table 6. Since Mar'ashi did not visit the inaccessible and rugged mountainous areas of the 'High-Alborz' and his report covers the lower valleys to the north and south of the epicentral area, his data is organized in Table 6 in two separate northern and the southern areas. The data in Table 6 indicates that the N–S width of the estimated intensity ~VIII area is over 40 km, extending from the Assassin castle of Pālisān of Rudbārāt-e-Alamut in the south to the Gorjiān and Golijān districts in the north. Daylamān, which suffered substantial damage during the earthquake, is located to the west-northwest of the meizoseissmal area. The distance between

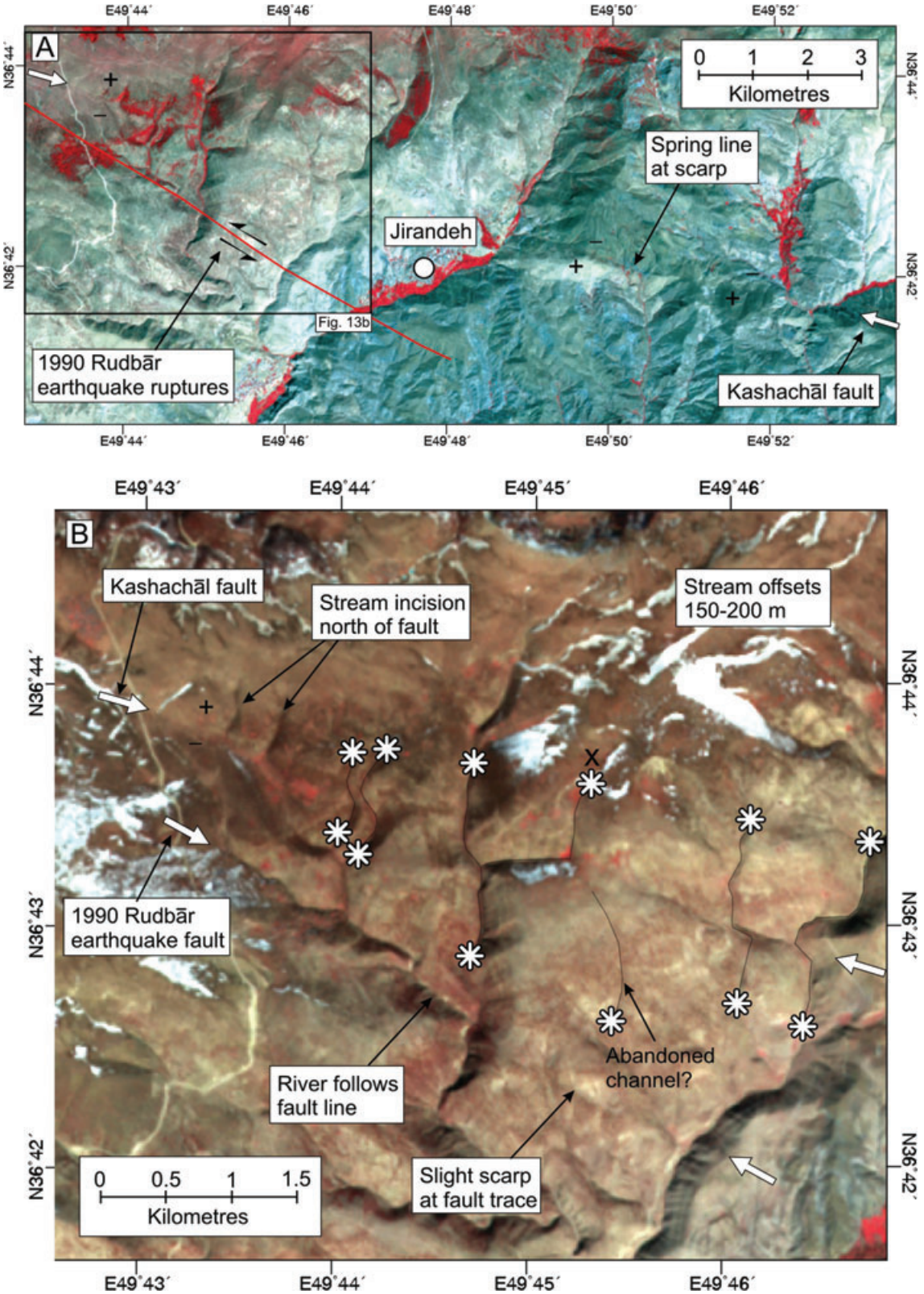

Figure 13. (a) ASTER image of the eastern part of the 1990 Rudbār rupture (red line) and the continuation to the east of the Kashachāl fault (trending between the white arrows). The two faults appear to diverge from a point situated close to the western limit of the Figure. The Kashachāl fault is marked by a series of north-facing scarps and a line of vegetation (spring line?). See Fig. 12a for the location. (b) Close-up ASTER image of the Rudbār and Kashachāl faults close to where they diverge (see part 'a' for location). The Kashachāl fault (trending between the white arrows) is clearer than the Rudbār fault, with a south-facing scarp, and showing a series of clear stream displacements of 150–200 m (ends of the streams are marked by white stars, see text for further details).

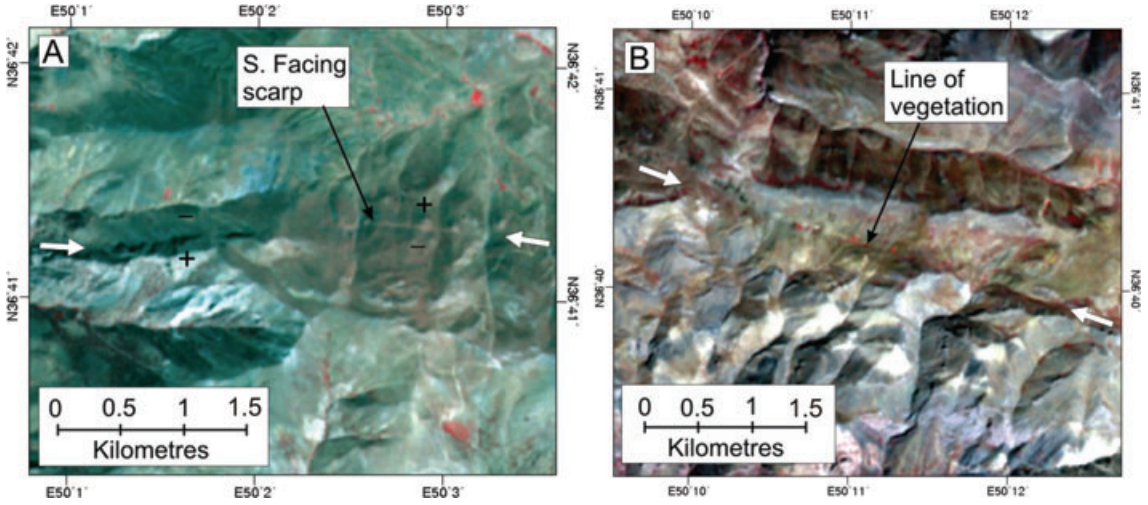

Figure 14. Close-up ASTER images of the Kashachāl fault (in both images the fault runs between the white arrows). In (a) the fault has a north-facing scarp in the west of the image and a south-facing scarp, which reverses the local topography, in the eastern part of the image. See Fig. 12(b) for the location In (b) the fault runs along a prominent linear valley marked by a series of patches of vegetation. See Fig. 12(b) for the location.

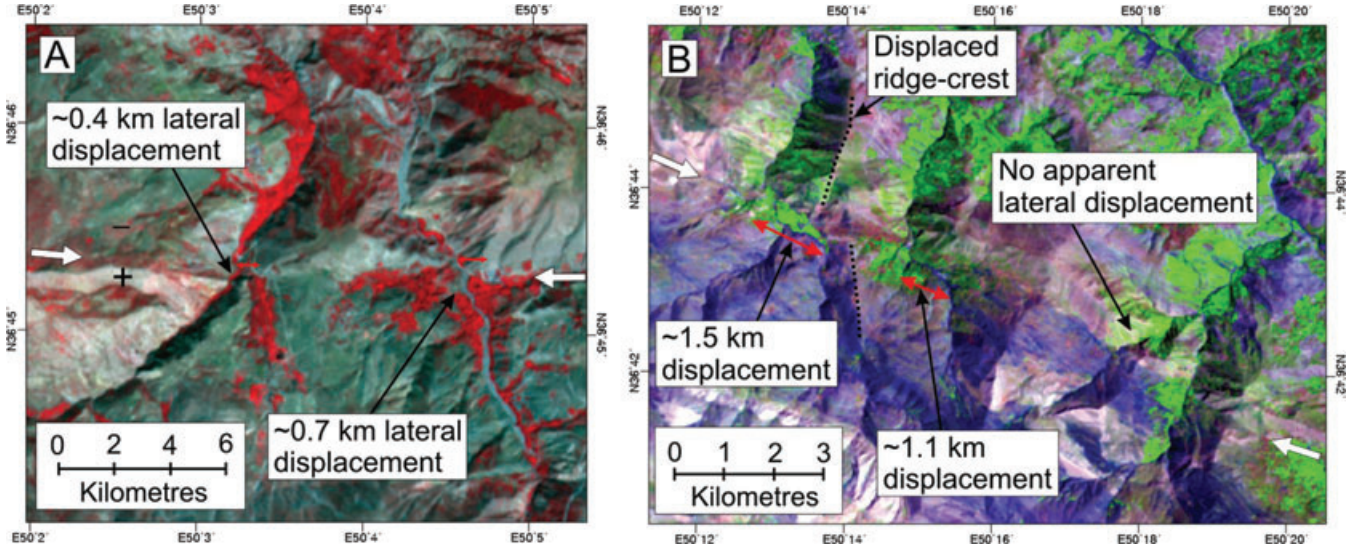

Figure 15. (a) Close-up ASTER image of the Kelishom fault showing two north-flowing rivers displaced by 0.4 km and 0.7 km (displacements are marked with red arrows). See Fig. 12(b) for the location. (b) LANDSAT image (RGB 5,4,1) of rivers crossing the Kelishom fault. The two rivers in the west, and the ridge-crest between them, are all displaced left-laterally by >1 km. The rivers in the east of the image show no lateral displacement. See Fig. 12(a) for the location.

Table 5. Summary of cumulative left-lateral displacements of the river courses cut by the Kelishom fault [organized from the west to the east (Figs 10a and 12a).

Designation [Fig. 6a]	Displaced riverbed location	Cumulative left-lateral displacement (km) (±100 m)
1	Chen [NW Kelishom; 36°45′–49°51′; +2084 m]	0.8
2	NNW Kelishom [36°46′–49°54′; +1981 m]	1.1
3	Pishkālijān [36°45′–50°03′; +1742 m]	0.4
4	Shāhijān, Lileh Chāk River [lit. Broken/faulted Lileh River; 36°45′–50°04′; +1783 m]	0.7
5	Varbon [Miyāvakh-bon River; 36°44′–50°07′; +1862]	1.2
6	Lesbo [36°43′–50°12′; +1985 m]	1.5
7	Bālidasht [36°43′–50°14′; +1947 m]	1.1
8	Kalrud [36°42′–50°17′; +2097 m]	?
9	Lashkān [Upper Polrud; 36°40′–50°21′; +1616 m]	?

Table 6. Summary of the 1485 August 15 [$I_o \sim$ IX, $M_s \sim 7.2$] upper polrud earthquake macroseismic data along the kelishom fault.

Location	Casualty	Earthquake destruction/damage	Estimated intensity
I. Northern Meizoseismal area data[a]			
Tonékābon [District between Upper Polrud & Upper Sehezār Valleys]		High buildings (palaces, mosques, & shrines) and public baths collapsed, the rest fissured	VIII
Shakvar [modern Eshkévar, Middle Polrud River area]	70	Many villages affected; old buildings collapsed	
Gorjiān [upper Chālakrud] River area and Golijān [lower Chālakrud River area]	106		VIII
Castle of Sardābsar in Gorjiān [lower Chālakrud River area]	2	Collapsed	VII
Jandeh Rudbār of Gorjiān [Jennat Rudbār of Chālakrud?]	–	A pig in panic leapt from top of mountain into river below and perished	
Daylamān [36.88°-49.90°; +1,449 m]	–	Many old buildings collapsed	VIII
Daylamestān [Daylamān area; Chākrud River area, west of Polrud River]	?	Numerous large rockfalls killed livestock	VIII
Rānku [lower Polrud area, south of Rudsar]	–	Strongly felt, minor damage. A part of an old palace fell down [possibly built by Seyyed Rāzikiyā in 820/1417 at Tamijān town, WSW of Rudsar (35.40°N- 37.20°E)]	VII
Hashtpar-e-Kohneh of Rānku	–	Partly collapsed	VII
Biyehpish [37.00°-49.60°]	–	Strongly felt, minor damage	VI
Lāhijān [37.20°-50.00°]	–	Strongly felt, minor damage	VI
Kissum [district between Lāhijān and Sefidrud]	–	Strongly felt, minor damage	VI
Gukeh [district between Lāhijān and Sefidrud, south of Kissum]	–	Strongly felt, minor damage	VI
Pāshijā [E. Sefidrud Delta]	–	Strongly felt, minor damage	VI
Lashteh-neshā [W. Sefidrud Delta]		Strongly felt, minor damage	VI
II. Southern Meizoseismal area data[a]			
Pālisān Castle [in Rudbārāt of Alamut; exact location unknown]	78		VIII
Rudbārāt [Alamutrud Valley, north of east Shāhrud-Alamutrud Rivers]	Many perished, number unknown		VIII

Note: [a]The width of intensity VIII between the northern and the southern meizoseismal area is over 40 km (Figs 10a and 12a).

Daylamān in the NW and Gorjiān [or Karjiyān according to Mostaufi (1340); the lower Chālakrud River] in the northeast is over 70 km (Table 6, Fig. 10a). Consequently, Mar'ashi's report, despite the lack of detailed information from the unapproachable and rugged 'High-Alborz', clearly indicates a large-magnitude earthquake with an elongated meizoseismal area stretching from the upper Polrud River in the SSE to the upper Chākrud River/Daylamān district in the NNW (Figs 4 and 10a, Table 6).

The Kelishom fault is the most obvious fault along the long axis of the 1485 meizoseismal area and shows apparent cumulative stream course displacements of > 1km (Figs 12a, 15a and b). We postulate that the Kelishom fault was ruptured during the 1485 August 15 large-magnitude earthquake. The destructive effect of the earthquake along the Kelishom fault bears resemblance with the Rudbār earthquake of 1990 June 20 along the Rudbār fault to the west of the 1485 epicentral area (Figs 10a and b). The meizoseismal area that we propose for the 1485 earthquake, therefore, assumes that the source faults have the same mechanism, comparable length, trend, and source dimensions, as well as being located in the same structural zone of the 'High-Alborz' (Figs 4, 5, 10a and b).

There are numerous first millennium B.C. archaeological sites along the Kelishom fault and some of them, such as Khoshkushān, Kelishom, Pishkāljān, Shāhijān and Darreh (Kāmbakhsh-Fard 1991), are in the close vicinity of the fault line (Fig. 4). It would be interesting to study these sites in the future to look for evidence of archaeoseismic events.

6.2 The 1608 April 20 Alamutrud earthquake [$I_o \sim$ X, $M_s \sim 7.6$]

The earthquake affected five villages of northeastern Qazvin where 3000 people were killed. The five villages are situated to the northwest of the four districts of Rudbārāt-e-Alamut known as Chāhār Kalāteh [lit., 'Four Forts' including: (i) Shams Kalāyeh; (ii) Mo'alem Kalāyeh, which is the centre of Alamut and Rudbārāt-e-Alamut District; (iii) Estalbar and (iv) Anādeh (possibly Nāveh); located about 36.45°N–50.48°E; Fig. 10a, Table 7]. Large landslides destroyed these villages and their inhabitants perished. For several days, 'bloody waters' were observed in the springs of Mo'alem Kalāyeh, which is located to the south of Chāhār Kalāteh, and was also destroyed. The village has been built on a large landslide of the red Neogene molasse and evidence of displacement on this landslide is still preserved at this locality. The castle of Darband [location unknown; possibly in southern Guilān] was also ruined. Some buildings were cracked and chimneys collapsed in Āmol [195 km to the NE], Sāri [230 km NE], and Ashraf [modern Behshāhr; 275 km NE] (Table 7 and Fig. 10a). The earthquake was strongly felt by Shāh 'Abbās Safavid [r. 1587–1628] and his hunting party at the Miyān Kāleh Peninsula royal hunting grounds of the southeast Caspian Sea, almost 300 km to the northeast of the epicentral area. The earthquake caused large sea waves in the Caspian Sea, and caused panic to people and cows, with the latter swimming out to the Caspian Sea (Monajem Yazdi, early 17th century; Sani' al-Dauleh

Table 7. Summary of the 1608 April 20 Alamutrud earthquake [$I_o \sim$ X, $M_s \sim 7.6$] limited macroseismic data along the Alamutrud fault fault (Fig. 10a).

Location	Coordinates (N–E)[a]	Earthquake destruction/damage	Estimated intensity
Darband Castle	[b]	Ruined	X
Five villages NW of Chāhār Kalāteh			
(i) Ovān	36°29′31″–50°27′01″; +1845 m.	Ruined, landslides	X
(ii) Varbon	36°29′14″–50°27′15″; +1882 m.	Ruined, landslides	X
(iii) Zarābād	36°29′23″–50°25′52″; +1789 m	Ruined, landslides	X
(iv) Zavārdasht	36°29′45″–50°25′56″; +1814 m.	Ruined, landslides	X
(v) 300 m N of Zavārdasht	[b]	Ruined, landslides	X
Chāhār Kalāteh			
(i) Shams Kālāyeh	36°27′–50°28′; +1700 m.	Ruined, landslides	X
(ii) Mo'alem Kālāyeh	36.26–40.28; 1541 m.	Ruined, landslides, springs w/red water	X
(iii) Estalbar	36°27′–50°28′; +1567 m.	Ruined, landslides	X
(iv) Anādeh [possibly Nāveh, south of Mo'alem Kālāyeh]	36°26′–50°28′; +1629 m.	Ruined, landslides	X
Caspian Sea Shore [50 km NNE]	Southern shore of the Caspian Sea	Seiche	VII
Damāvand [150 km SE]	35°43′–52°04′; +1964 m	Repair of the Jame' Mosque [inscription dated 1615].	Possibly associated w/the 1608 eq. damage
Āmol [195 km NE]	36°28′–52°20′; +87 m.	Chimneys collapsed, buildings fractured.	VI
Sāri [230 km NE]	36°33′–53°03′; +38 m.	Buildings fractured	V
Ashraf [modern Behshahr; 275 km NE]	36°41′–53° 32′; +30 m.	Buildings fractured	V
Miyān Kāleh Peninsula [300 km NE]	SE Caspian Sea	Strongly felt	IV+
Shamakhi [500 km NW]	40°38′–48°38′; +705 m	Felt	IV

Notes: [a]Due to proximity of some small sites, an exact coordinate is given.
[b]Location unknown.

1919; Golriz 1958; Meshkāti 1970; 'Asgari 1971; Ambraseys & Melville 1982; Berberian *et al.* 1983; Berberian 1994).

The Chāhār Kalāteh villages are located on a large mass of landslide with large blocks of rock avalanche to its north [1.0 × 3.5 km]. On this landslide/rock avalanche mass, there are at least three particular mound-like areas with visible traces of old demolished houses. These destroyed old villages, visible on aerial photographs and satellite imagery, are located to the NW [36.45°N–50.46°; 1659 m] and SW [36.43°N–50.46°; 1535 m] of Mo'alem Kalāyeh, and WSW of Nāveh [south of Mo'alem Kalāyeh; 36.43°–50.46°; 1496 m]. These mounds are remnants of the villages destroyed during the 1608 earthquake.

The unnamed five destroyed villages NW of Chāhār Kalāteh could be those located about four to six km NW of Mo'alem Kalāyeh near the confluence of the two rivers of Avān and Kudareh [Avān, Varbon, Zarābād, Zavārdasht, and a village 300 m north of the latter; see Table 7]. These five villages are also located in a landslide/rockfall terrain with a small lake formed in between them [Avān Lake; 36.45°–50.43°; 1806 m]. To the immediate west of Varbon and SW of Avān villages in the Avān valley, a large mound is visible on aerial photographs and satellite imagery with old ruined houses [36.48°–50.43°; 1821 m]. The three villages to the west located in the Kudareh valley [Zarābād, Zavārdasht, and a village 300 m north of the latter] are surrounded and covered by dense trees and cannot be assessed through remote-sensing. The unconstrained meizoseismal area of the 1608 earthquake (Fig. 10a and Table 7) may suggest that the Alamutrud reverse fault could be a likely source of the event.

7 CONCLUSIONS

Our aims in writing this paper have been two-fold. First, we provide a clearer description of the Rudbār earthquake; one of the worst seismic disasters to have struck Iran in the modern period. This description has included many details that have not been published elsewhere. We have also attempted to place the Rudbār earthquake in the context of both historical large-magnitude events, and the late Cenozoic history of active strike-slip faulting within the 'High-Alborz' Mountains.

The earthquake was associated with 80 km NW–SE trending left-lateral strike-slip faulting, parallel to the high mountain belt of intense folding, reverse faulting and nappe structures. The coseismic surface faulting, which occurred on a previously unknown fault with subtle geomorphic expression, showed unusual larger vertical displacement in the opposite sense of the existing topography. It was composed of at least three right-stepping strike-slip segments which did not cross the transverse Sefidrud deep gorge, possibly indicating a deep structural discontinuity along the gorge. All the modelling agrees with a bilateral rupture propagation with shorter rupture propagation to the northwest and longer one to the southeast. The northwestern segment, to the west of the initial rupture zone, showed slight displacement with minor normal component. The middle and the southeastern segments revealed larger displacements with minor reverse component. The pre-1990 earthquake topography, which provided no clear evidence of the last similar slip event, indicates that the last major rupture along the Rudbar fault may have been several thousand years ago.

Locally recorded aftershocks showed more activity in the southeast than in the northwest. Teleseismically recorded aftershocks with strike-slip and reverse mechanisms covered a large area far beyond the coseismic surface strike-slip fault zone. The majority of the aftershocks took place to the north and NW of the surface rupture, and some clustered in the major gap at the Sefidrud gorge and the southeastern extremity of the fault. Roughly N–S thrust aftershocks were located at the southeastern extremity of the surface rupture as well as in the Sefidrud deep gorge. These aftershocks

seem to be associated with activity of thrust splay faults associated with the terminations of strike-slip segments.

The Alborz Mountains of northern Iran accommodates the overall motion between the Southern Caspian and Central Iran, and seems to involve oblique left-lateral shortening. The rather small cumulative left-lateral displacements observed along the Rudbār fault suggest that the onset of faulting in this region of the High-Alborz is relatively recent and is likely to long postdate the onset of mountain building of the Alborz which is recorded ∼5 Ma by apatite (U-Th)/He (Rezāeian 2008). The 1990 Rudbar fault is one of the three range-parallel left-lateral strike-slip faults with indications of recent activity. Apparent left-lateral displacements on the nearby Kelishom and Kashachāl faults mark them out as potential eastward continuations of the active Rudbār earthquake fault. These two faults are, therefore, potential sources of future large-magnitude earthquakes and should be the subject of further, detailed, research.

ACKNOWLEDGMENTS

We thank the Geological Survey of Iran for the field support. MB's research for this work was not supported by any grant or organization. RTW is supported by a University Research Fellowship from the Royal Society. Jean Franço Ritz is thanked for discussions on the Kelishom fault. J. Elliott is acknowledged for help in drafting Fig. 6, and Christine Johnson and Enny Aminiān for Figs 4 and 5. We appreciate the constructive reviewer comments of Denis Hatzfeld and Glenn Biasi.

REFERENCES

Allen, M.B., Ghassemi, M.R., Shahrabi, M. & Qorashi, M., 2003. Accomodation of late Cenozoic oblique shortening in the Alborz range, northern Iran, *J. Struct. Geol.,* **25,** 659–672.

Ambraseys, N.N., 1974. Historical seismicity of North-Central Iran. In: Materials for the study of seismotectonics of Iran; North Central Iran, *Geol. Surv. Iran, Rep.,* **29,** 47–95.

Ambraseys, N.N., 1978. The relocation of earthquakes in Iran, *Geophys. J.R. Astr. Soc.,* **53,** 117–121.

Ambraseys, N.N., 2001. Reassessment of earthquakes, 1900–1999, in the Eastern Mediterranean and the Middle East, *Geophys. J. Int.,* **145,** 471–485.

Ambraseys, N.N. & Melville, C., 1982. *A History of Persian Earthquakes,* Cambridge University Press, Cambridge, 219p.

Anders, M.H. & Schlische, R.W., 1994, Overlapping faults, intrabasin highs, and the growth of normal faults, *J. Geol.,* **102,** 165–179.

Anklesaria, B.T., 1956. Zand-Akasih; Iranian or Greater Bundahishn. English transliteration and translation, Bombay. Digital version by J.P. Peterson available at http://www.avesta.org/mp/grb.htm.

Annells, R.N., Arthurton, R.S., Bazley, R.A.B., Davis, R.G., Hamedi, M.A.R. & Rahimzadeh, F., 1985a. Geological quadrangle map of Qazvin, 1:250,000, *Geol. Surv. Iran,* E3.

Annells, R.N., Arthurton, R.S., Bazley, R.A.B., Davis, R.G., Hamedi, M.A.R. & Rahimzadeh, F., 1985b. Geological quadrangle map of Rasht, 1:250,000, *Geol. Surv. Iran,*E4.

Arrowsmith, J.R. & Rhodes, D.D., 1994. Original forms and initial modifications of the Galway Lake Road Scarp formed along the Emerson fault during the 28 June 1992 Landers, California, earthquake, *Bull. seism. Soc. Am.,* **84**(3), 511–527.

'Asgari, A.B., 1971. *Behshahr (Ashraf al-Belād),* Iran Chap Publ., Tehran, 1350 (in Persian).

Āstaneh, A. & Ghafory-Ashiāny, M., 1990. The Manji, Iran, earthquake of June 21, 1990, *EERI Newslett.,* **24**(12), 5–12.

Berberian, M., 1979. Evaluation of the instrumental and relocated epicentres of Iranian earthquakes, *Geophys. J. R. astr. Soc. Lond.,* **58,** 625–630.

Berberian, M., 1981. Active faulting and tectonics of Iran, in *Zagros-Hindu Kush-Himalaya Geodynamic Evolution,* pp. 33–69, eds Gupta H.K. and Delany F.M., Am. Geophys. Union, Geodyn. Series 3.

Berberian, M., 1983. The southern Caspian; a compressional depression floored by a trapped, modified oceanic crust, *Can. J. Earth Sci.,* **20,** 163–183.

Berberian, M., 1994. *Natural Hazards and the first earthquake catalogue of Iran*. Vol. 1: Historical Hazards in Iran Prior to 1900, International Institute of Earthquake Engineering and Seismology, Tehran, 603 p. in English & 66 p. in Persian.

Berberian, M., 1997. Seismic sources of the transcaucasian historical earthquakes, in *Historical and Prehistorical Earthquakes in the Caucasus,* Vol. 28, pp. 233–311, eds Giardini, D. & S. Balassanian, NATO ASI Series, 2. Environment,-, Kluwer Academic Press, The Netherlands.

Berberian, M., 2005. The 2003 Bam urban earthquake: a predictable seismotectonic pattern along the western margin of the rigid Lut Block, southeast Iran, *Earthq. Spectra,* **21**(S1), S35–S99. Earthquake Engineering Research Institute. doi:10.1193/1.2127909.

Berberian, M. & Qorashi, M., 1984. Recent tectonics, seismotectonics and earthquake-fault hazard study of the Zanjan Lead-Zinc Melting Plant, *Geol. Surv. Iran, Int. Rep.,* 88p (in Persian).

Berberian, M. & Yeats, R.S., 1999. Patterns of historical rupture in the Iranian Plateau, *Bull. seism. Soc. Am.,* **89**(1), 120–139.

Berberian, M. & Yeats, R.S., 2001. Contribution of archaeological data to studies of earthquake history in the Iranian Plateau. Paul Hancock Memorial Issue, *J. Struct. Geol.,* **23,** 536–584.

Berberian, M., Qorashi, M., Arzhangravesh, B., & Mohajer-Ashjai, A., 1983. Recent tectonics, seismotectonics and earthquake-fault hazard study in the Greater Qazvin region, *Geol. Surv. Iran,* **57,** 84p. (in Persian).

Berberian, M., Qorashi, M., Arzhangravesh, B. & Mohajer-Ashjai, A., 1985. Recent tectonics, seismotectonics and earthquake-fault hazard study in the Greater Tehran area, *Geol. Surv. Iran,* **56,** 316p. (in Persian).

Berberian, M., Qorashi, M., Jackson, J.A., Priestley, K. & Wallace, T., 1992. The Rudbar-Tarom earthquake of June 20, 1990 in NW Persia: Preliminary field and seismological observations, and its tectonic significance, *Bull. seism. Soc. Am.,* **82,** 1726–1755.

Berz, G., 1992. Losses in the range of US$ 50 billion and 50,000 people killed: Munich Re's list of major natural disasters in 1990, *Nat. Hazards,* **5,** 95–102.

Campos, J., Madariaga, R., Nabelek, J., Bukchin, B.G. & Deschams, A., 1994. Faulting process of the 1990 June 20 Iran earthquake from broadband records, *Geophys. J. Int.,* **118,** 31–46.

Choy, G. & Zednik, J., 1997. The rupture process of the Manjil, Iran earthquake of June 20 1990 and implications for intraplate strike-slip earthquakes, *Stud. Geophys. et Geod.,* **41,** 45–63.

Cockerham, R.S. & Corbett, E.J., 1987. The July 1986 Chalfant Valley, Clifornia, earthquake sequence: preliminary results, *Bull. seism. Soc. Am.,* **77,** 280–289.

Dashti, Gh., 1990. The responsible fault of the June 20, 1990 earthquake, in *Proceedings of the free Conference on June 20, 1990 Gilan-Mazandaran earthquake*, 11–12 August 1990, Building and Housing Research Center, Tehran.

Dewey, J.W., 1971. Seismicity studies with the method of joint hypocenter determinations, *PhD thesis,* University of California, Berkeley, 164p.

Dewey, J.D., 1983. Relocation of instrumentally recorded pre-1974 earthquakes in the South Carolina region, in *Studies Related to the Charlestone, South Carolina, Earthquake of 1886,* ed. Gohn, G.S., U.S. Geol. Surv. Prof. Paper 1313, Q1-Q9.

Dziewonski, A.M., Ekstom, G., Woodhouse, J.H. & Zwart, G., 1991. Centroid-moment tensor solutions for April-June 1990, *Phys. Earth planet. Inter.,* **66,** 133–143.

Dziewonski, A.M., Ekstom, G. & Salganik, M.P., 1992. Centroid-moment tensor solutions for October-December 1991, *Phys. Earth planet. Inter.,* **74,** 89–100.

Engdahl, E.R., Van Der Hilst, R. & Buland, R., 1998. Global teleseismic earthquake relocation with improved travel times and procedures for depth determination, *Bull. seism. Soc. Am.,* **88,** 722–743.

Engdahl, E.R., Jackson, J.A., Myers, S.C., Bergman, E.A. & Priestley, K., 2006. Relocation and assessment of seismicity in the Iran region, *Geophys. J. Int.,* **167,** 761–778.

Eslami, A.A., 1992. An illustration of the June 1990 Rudbar earthquake fault system, *Geosci., Geol. Surv. Iran,* **2**(5), 48–53 (in Persian)

Farr, T. & Kobrick, M., 2000. Shuttle Radar Topographic Mission produces a wealth of data, *EOS, Trans. Am. geophys. Un.,* **81,** 583–585.

Gao, L., 1993. Seismotectonics, fault mechanics inferred from seismic body wave inversion, *PhD thesis*, University of Arizona, Tucson, 173p.

Gao, L. & Wallace, T.C., 1995. The 1990 Rudbar-Tarom Iranian sequence: evidence for slip partitioning, *J. geophys. Res.,* **100,** 15 137–15 332.

Gao, L., Wallace, T.C. & Jackson, J.A., 1991. Aftershocks of the June 1990 Rudbar-Tarom earthquake: Evidence for slip partitioning (Abstract), *EOS, Trans. Am. geophys. Un.,* **72**(44), Fall Meeting suppl. 335.

Ghalamghāsh, J. & Rashid, H., 2002. Geological Sheet of Jirandeh, 1:1,00,000, *Geol. Surv. Iran*, **5963**.

Giardini, D., Malagnini, L., Palombo, B. & Bosch, E., 1994. Broad-band moment tensor inversion from single station, regional surface waves for the 1990, NW-Iran earthquake sequence, *Annali di Geofisica,* **XXXVII**(6), 1645–1656.

Golriz, M.A., 1958. *Minudar ya Bal al-Jennat-e-Qazvin [The Paradise Gate of Qazvin],* Tehran University Publ. 447, pp. 1337 (in Persian).

Guest, B., Stockli, D.F., Grove, M., Axen, G.J., Lam, P.S. & Hassanzadeh, J., 2006. Thermal Histories from the central Alborz Mountains, northern Iran: Implications for the spatial and temporal distribution of deformation in northern Iran, *Geol. Soc. Am. Bull.,* **118**(11/12), 1507–1521.

Haerinck, E., 1989. The Archaemenid (Iron Age IV) period in Gilan, Iran, in *Archaeologia Iranica et Orientalis, Miscellanea in Honorem Louis Vanden Berghe,* Vol. I, pp. 455–473, eds De Meyer, L. & E. Haerinck, Peeters Press, Belgium.

Haghshénās, E., 1998. Geotechnical aspects overview of the Manjil earthquake north of Iran (20 June 1990), in *Proceedings of the 1st Iran-Japan Workshop Recent Earthquakes in Iran & Japan*, May 16–18, 1998, Tehran, pp. 171–183.

Hākemi, A., 1968. Kaluraz and the civilization of the Mardes, *Archaeologia Viva,* **1**(1), 63–65.

Hamzehloo, H., Sarkar, I. & Chander, R., 1997a. Analysis of some aftershocks of the Rudbar earthquake of 1990 using master event technique, *Bull. Indian Soc. Earthq. Techno.,* **33,** 1–16.

Hamzeloo, H., Chander, R. & Sarkar, I., 1997b. Probable role of the Sefirud reservoir in the occurrence of the Rudbar earthquake of 1990, *Bull. Ind. Soc. Tech.,* **34,** 17–25.

Hollingsworth, J., Jackson, J., Walker, R., Gheitanchi, M. & Bolourchi, M., 2006. Strike-slip faulting, rotation, and along-strike elongation in the Kopeh Dagh mountains, NE Iran, *Geophys. J. Int.,* **166,** 1161–1177.

Ichinose, G.A., Smith, K.D. & Anderson, J.G., 1998. Moment tensor solutions of the 1994 to 1996 Double Spring Flat and implications for local tectonic models, *Bull. seism. Soc. Am.,* **88**(6), 1363–1378.

Ishihara, K., Haeri, M., Moinfar, A.A., Towhata, I. & Tsujino, S., 1992. Geotechnical aspects of the June 20, 1990 Manjil earthquake in Iran, *Soils Found.,* **32**(3), 61–78 (Japanese Society of Soil Mechanics and Foundation Engineering).

Jackson, J.A. & McKenzie, D.P., 1984. Active tectonics of the Alpine-Himalayan belt between western Turkey and Pakistan, *Geophys. J. R. astr. Soc.,* **77**, 185–264.

Jackson, J. & McKenzie, D., 1985. Rotational mechanisms of active deformation in Greece and Iran, in: *Tectonics of the Mediterranean, Spl. Pub. Geol. Soc., London* **17**, pp. 743–754.

Jackson, J.A. & McKenzie, D.P., 1988. The relationship between plate motions and seismic moment tensor, and rates of active deformation in the Mediterranean and Middle East, *Geophys. J. R. astr. Soc.,* **93,** 45–73.

Jackson, J., Priestley, K., Allen, M. & Berberian, M., 2002. Active tectonics of the South Caspian Basin, *Geophys. J. Int.,* **148**(2), 214–245.

Johnson, A.M., Fleming, R.W. & Gruikshank, K.M., 1994. Shear zones formed along long, straight Traces of fault zones during the 28 June 1992, Landers, California, Earthquake, *Bull. seism. Soc. Am.,* **84**(3), 499–510.

Kāmbakhsh-Fard, S., 1991. *3,200 years Old Tehran based on archaeological investigations, Fazā Publ.*, 212 pp., (in Persian).

Māheri, M.R., 1991. Response of large structure to Manjil earthquake of June 1990, in *Proceedings of the 1st Int. Conf. Sesim. & Eq. Engin., IIEES,* Tehran, May 27–29, 1991, Vol 2, pp. 1019–1028.

Mar'ashi, Sayyed Zahir al-Din, 1489. Tarikh-e-Gilan va Daylamestan [The History of Gilan and Daylamestan (Mazandaran)]. H.L. Rabino, *Rasht*, 1330/1912. Ed. Manuchehr Sotudeh, Tehran, 1347/1968 (in Persian).

McKenzie, D.P. & Jackson, J.A., 1983. The relationship between strain rates, crustal thickening, paleomagnetism, finite strain, and fault movements within a deforming zone. *Earth planet. Sci. Lett.,* **65,** 182–202.

Meshkāti, N., 1970. Historical Monuments and Archaeological Sites in Iran. *Sāzemān Melli Hefāzat Āthār Bāstāni Irān,* **1,** 370p, Tehran (in Persian).

Moinfar, A.A. & Naderzadeh, A., 1990. An immediate and preliminary report on the Manjil, Iran earthquake of June 20, 1990, Building and Housing Research Center, Ministry of Housing and Urban Development, **119**, 57 p. (in Persian w/11 p. in English).

Monajem Yazdi, Jalal al-Din Mohammad, *Early 17th century. Tarikh-I 'Abbasi,* Tehran University Library, **4204**, Tehran.

Nabavi, M.S., 1972. Seismicity of Iran, *M.Ph. thesis*. University of London.

Nazari, H. & Salāmati, R., 1998. Geological sheet of Rudbar, 1:100,000, *Geological Survey of Iran,* **5863**.

Negahbān, E.O., 1968. Marlik, a royal necropolis of the second millennium, *Archaeologia Viva,* **1**(1), 59–62.

Negahbān, E.O., 1990. Silver vessel of Marlik with gold spout and impressed gold designs, *Iranica Varia,* **XVI,** 144–151.

Niāzi, M. & Bozorgniā, Y., 1992. The 1990 manjil, Iran, earthquake: geology and seismology overview, PGA attenuation, and observed damage, *Bull. seism. Soc. Am.,* **82,** 774–799.

Priestley, K.F., Baker, C., & Jackson, J.A., 1994. Implications of earthquake focal mechanism data for the active tectonics of the South Caspian Basin and surrounding regions, *Geophys. J. Int.,* **118,** 111–141.

Rabino, H.L., Di Borgomale, 1928. Mazandaran and Astarabad. E.F.W. Gibb Memorial New Series, Vol. VII, *Luzac & Co.*, London, 171 p. in English & 235 p. in Persian/Arabic. Also: Persian Translation by Gholam 'Ali Vahid Mazandarani, *Sherkat Entesharat 'Elmi va Farhangi*, Tehran, 1336/1957, 371p. (in Persian).

Ramazi, H.R., 1991. Seismotectonics of the 1990 Manjil-Rudbar earthauke. In Analytical report No. 1; the Manjil-Rudbar earthquake (Iran), Khordad 31, 1369 [June 20, 1990], *IIEES,* Tehran, **70–91-1,** 32–44 (in Persian).

Rezāeian, M., 2008. Coupled Tectonic, Erosion and Climate in the Alborz Mountains, Iran, *PhD thesis*, University of Cambridge.

Rezāpour, M., 1991. Aftershocks study of Manji-Rudbar earthquake of June 20, 1990, *MSc thesis*, Institute of Geophysics, Tehran University (in Persian).

Ritz, J.-F., Nazari, H., Ghassemi, A., Salamati, R., Shafei, A., Solaymani, S. & Vernant, P., 2006. Active transtension inside central Alborz: a new insight into northern Iran-southern Caspian geodynamics, *Geology,* **34,** 477–480.

Sani' al-Dauleh, M.H., 'Etemad al-Saltaneh, 1919. *Montamzam-e-Naseri [Chronicles of the Naser al-Din Shah Period]*. 3 vols., 1298–1300-1880–82, Lith. Print, Tehran (in Persian).

Sarkār, I., Hamzehloo, H. & Khattri, K.N., 2003. Estimation of causative fault parameters of the Rudbar earthquake of June 20, 1990 from near filed SH-wave data, *Tectonophysics,* **364,** 55–70.

Skovorodkin, Yu., Guseva, T. & Bezuglaya, L., 1999. Post seismic deformation and geomagnetic variation in epicentral area of the Rudbar earthquake of 1990, in *Proceedings of the 3rd Int. Conf. Seism. Earthq. Engineer.*, *IIEES*, May 17–19, 1999, Tehran, pp. 79–84.

Sotudeh, M., 1968. *Az Āstārā tā Astarābād [Form Āstārā to Astarābād],* 2 vols. Tehran. Also 1970, 1972, &1978 eds.

Stocklin, J. & Eftekhārnezhād, J. (compilers) 1969. Geological quadrangle map of Zanjān, 1:250,000, *Geological Survey of Iran*, **D4**.

Tatar, M., 2001. Etude sismotectonique de deux zones de collision continentale: le Zagros et l'Alborz (Iran), *thesis* L'Universite Joseph Fourier-Grenoble I, France, pp. 144–258.

Tatar, M. & Hatzfeld, D., 2009. Microseismic evidence of slip partitioning for the Rudbar-Tarom earthquake (Ms 7.7) of 1990 June 20 in NW Iran, *Geophys. J. Int.,* **176,** 529–541, doi:10.1111/j.1365-246X.2008.03976.x.

Thio, H.K., Satake, K., Kikuchi, M. & Kanamori, H., 1990. On the Sudan, Iran, and Philippines earthquakes of 1990 (abstract), *EOS, Trans. Am. geophys. Un.,* **71,** 1438.

Tsukuda, T. *et al*., 1991. Aftershock distribution of the 1990 Rudbar, northwest Iran, earthquake of M 7.3 and its tectonic implications, *Bull. Earthq. Res. Inst. Univ. Tokyo,* **66,** 351–381.

Underwood, C.R., 1991. Social and cultural factors in earthquake preparedness and response: Public health lessons from the 1990 earthquake in Iran, in *Proceedings of the 1st Int. Conf. Seism. & Earthq. Engineer., IIEES,* Vol. 2, pp. 1237–1244, 1991 May 27–29, Tehran.

UNDRO, 1990a. Iran-Earthquake, UNDRO Information Report No. 1 (June 21, 1990). through No. 14 (July 18, 1990). United Nations Department of Humanitarian Affairs (DHA), (http://www.reliefweb.int/rw/RWB.NSF/db900SID/OCHA-64DFLY?OpenDocument).

UNDRO, 1990b. Iran Earthquake, *UNDRO New,* July/August 1990, Geneva, Switzerland, pp. 4–8.

UNDRO, 1990c. Iran Earthquake: master plan for reconstruction, *UNDRO News*, September/October 1990, Geneva, Switzerland, pp. 4–6.

Vernant, P., *et al*., 2004. Present-day crustal deformation and plate kinematics in Middle East constrained by GPS measurements in Iran and north Oman, *Geophys. J. Int.,* **157,** 381–398.

Virieux, J., Deschamps, A., Perrot, J. & Campos, J., 1994. Source mechanisms and near-source wave propagation from broadband seismograms, *Annali di Geofisica,* **XXXVII**(6), 1565–1590.

Zāre', M., 1991a. The seismotectonic study of the reconstruction of the Sefid-Rud dam with special reference to the earthquake of 20th June 1990, Manjil NW of Iran, in *Proceedings of the 1st Int. Conf. on Seism. & Earthq. Engineer. SSE-1, IIEES,* Vol. 1, pp. 85–93, May 27029, 1991.

Zāre', M., 1991b. The seismotectonic and neotectonic analysis of the reconstruction operation of the Sefid Rud dam, with special reference to the earthquake of 20th June 1990, Manjil, Noeth-West of Iran, in *Proceedings of the 5th Int. Conf. Soil Dynamics & Earthq. Engineer.*, Karlsruhe, Germany, **2**. Computational Mechanics Publication, Southampton.

Zāre', M., 1995. Nonlinear soil behavior in the near-field; a case-study on the recent Iranian accelerometric data, in *Proceedings of the 2nd Int. Conf. Seism. Eq. Eng., IIEES*, May 14–17, 1995, pp. 1283–1292.

Zāre', M. & Moinfar, A.A., 1993. Earthquake fault induced landslide during the Manji, Iran (1990) earthquake, in *Proceedings of the 8th Int. Seminar Earthq. Prognostics,* Vol. 1, pp. 39–40. National Disaster Prevention Center of Iran, Tehran.

Zāre', M. & Moinfar, A.A., 1994. Comment on "The Rudbar-Tarom earthquake of 20 June 1990 in NW Persia: a preliminary field and seismological observations and its tectonic significance" by M. Berberian, M. Qorashi, J.A. Jackson, K. Priestely, and T. Wallace, *Bull. seism. Soc. Am.,* **84**(2), 484–485.

ZUR-RMT. Zurich Moment Tensor. Swiss Seismological Service.